ISOLDE Workshop and Users meeting 2023

Istituto per la Microelettronica e Microsistemi

Consiglio Nazionale delle Ricerche

Development of large-area topological insulators for spintronics

Roberto Mantovan
CNR-IMM Unit of Agrate Brianza
https://unit.mdm.imm.cnr.it/users/mantovan-roberto
roberto.mantovan@cnr.it

www.imm.cnr.it

Team

Dr. Roberto Mantovan

Dr. Emanuele Longo

Dr. Lorenzo Locatelli

The **Institute for Microelectronics and Microsystems** is one of the largest research institutes of the **CNR - National Research Council**

Dr. Claudia Wiemer

Dr. Matteo Belli

Mr. Mario Alia

SKYTOP
Skyrmion-Topological insulator and Weyl semimetal technology

https://skytop-project.eu/
(2018-2023)

Former members:
Dr. Massimo Longo (now at IMM Rome)
Dr. Raimondo Cecchini (now at IMM Bologna)
Dr. Martino Rimoldi (now at CERN)

Main collaborations:
Univ. Milano-Bicocca (Prof. Marco Fanciulli)
Demokritos, Athens (Prof A. Dimoulas)

Summary

- **Motivation**
  - Topological insulators: intro and applications

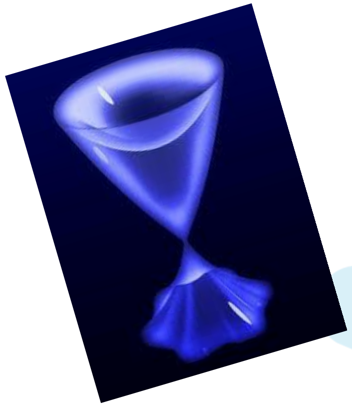

- **MOCVD of topological insulators**
  - Sb_2Te_3, Bi_2Te_3 and Sb_2Te_3/Bi_2Te_3 on large-area Si-based substrates

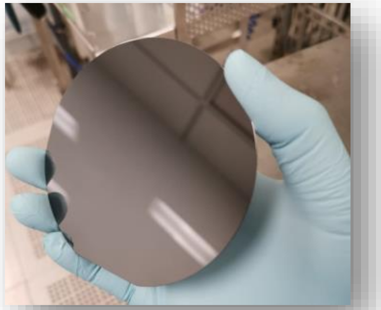

- **Spin-charge conversion in MOCVD-TIs**
  - The case of Sb_2Te_3 and Sb_2Te_3/Bi_2Te_3

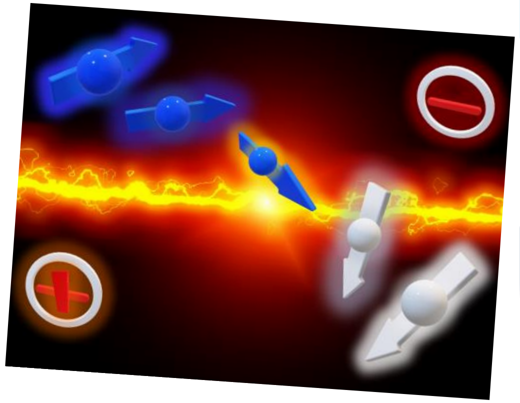

- **Conclusions & Outlook**

Our general aim

Spintronics

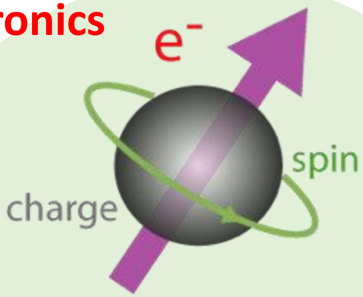

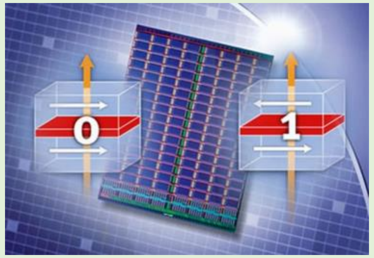

Topological Matter

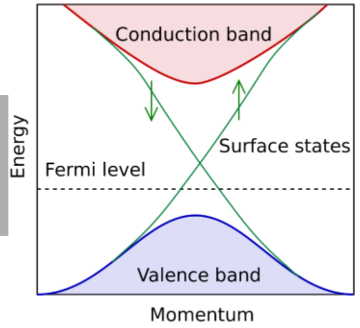

An «eye open» on technology transfer…

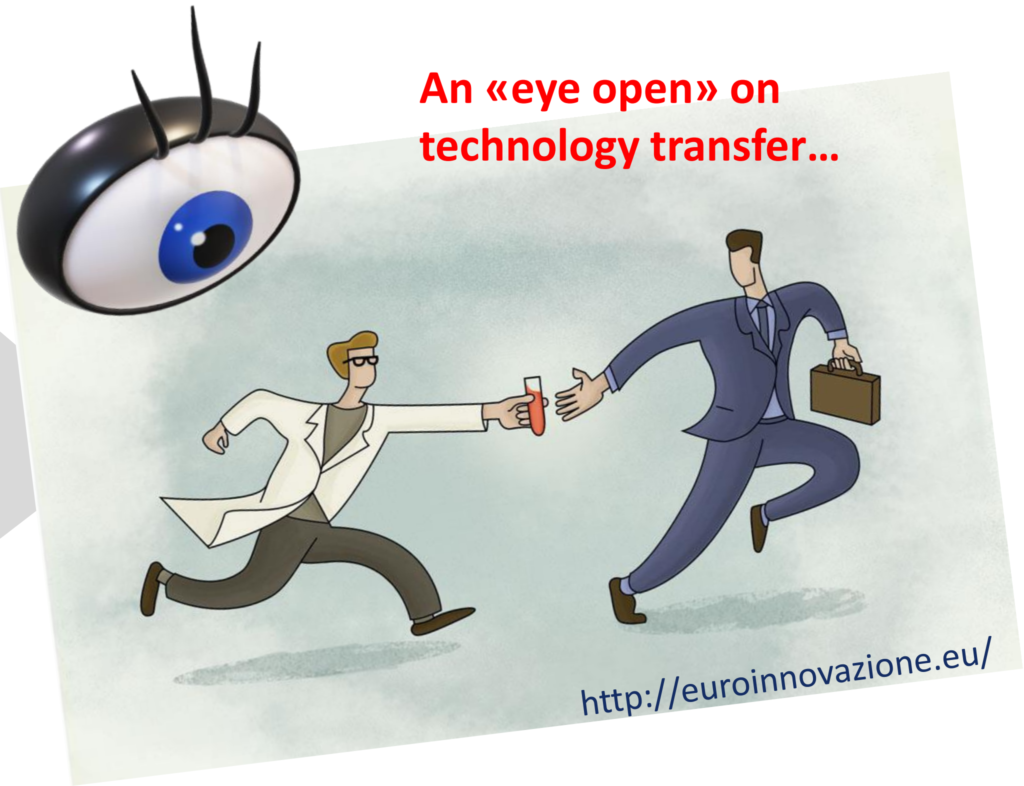

Timeline in topological

The Nobel Prize in Physics 2016

The Royal Swedish Academy of Sciences has decided to award the Nobel Prize in Physics 2016 with one half to

David J. Thouless

University of Washington, Seattle, WA, USA

and the other half to

F. Duncan M. Haldane and **J. Michael Kosterlitz**

Princeton University, NJ, USA

Brown University, Providence, RI, USA

"for theoretical discoveries of topological phase transitions and topological phases of matter"

They revealed the secrets of exotic matter

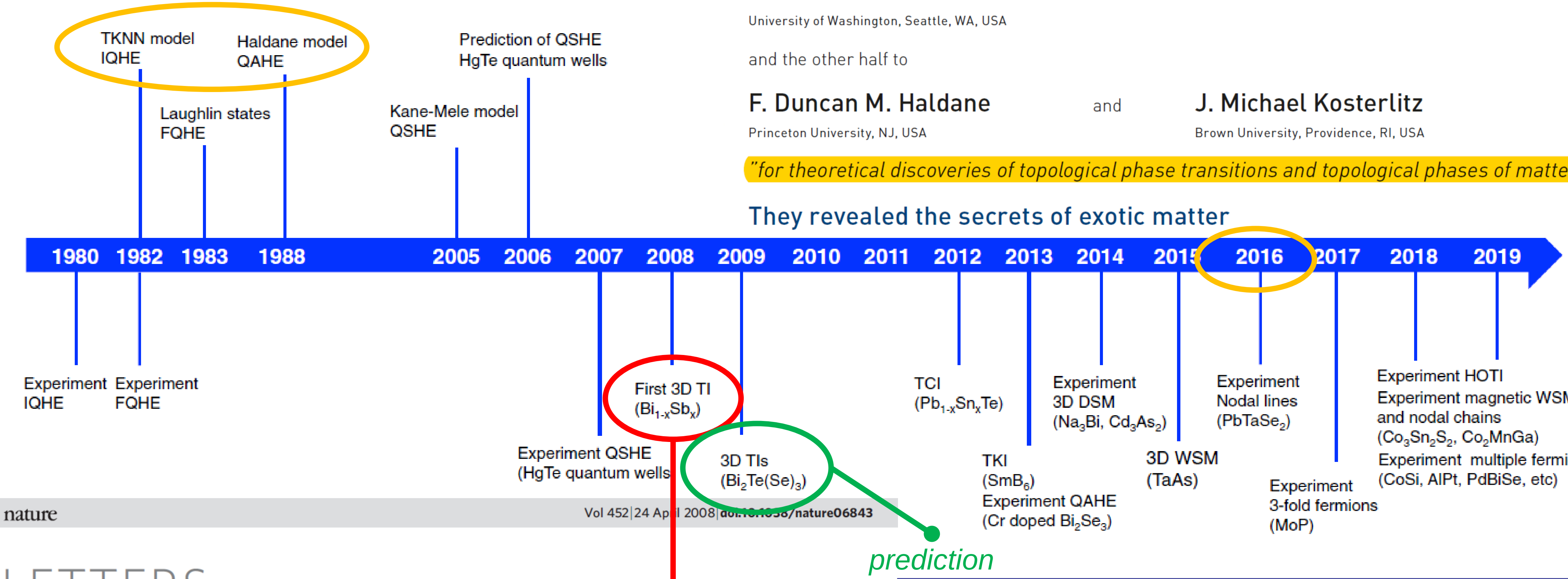

nature Vol 452|24 April 2008|doi:10.1038/nature06843

LETTERS

A topological Dirac insulator in a quantum spin Hall phase

D. Hsieh[1], D. Qian[1], L. Wray[1], Y. Xia[1], Y. S. Hor[2], R. J. Cava[2] & M. Z. Hasan[1,3]

ARTICLES
PUBLISHED ONLINE: 10 MAY 2009 | DOI: 10.1038/NPHYS1270
nature physics

Topological insulators in Bi_2Se_3, Bi_2Te_3 and Sb_2Te_3 with a single Dirac cone on the surface

Haijun Zhang[1], Chao-Xing Liu[2], Xiao-Liang Qi[3], Xi Dai[1], Zhong Fang[1] and Shou-Cheng Zhang[3]*

3D - TI

Bi_2Se_3, Bi_2Te_3, Sb_2Te_3 and Sb_2Se_3 share the same **rhombohedral crystal structure** with the space group D^5_{3d} *(R3̄m)* with five atoms in one unit cell (→ **quintuple layer, QL**)

ARTICLES
PUBLISHED ONLINE: 10 MAY 2009 | DOI: 10.1038/NPHYS1270
nature physics

2009, prediction

Topological insulators in Bi_2Se_3, Bi_2Te_3 and Sb_2Te_3 with a single Dirac cone on the surface

Haijun Zhang[1], Chao-Xing Liu[2], Xiao-Liang Qi[3], Xi Dai[1], Zhong Fang[1] and Shou-Cheng Zhang[3]*

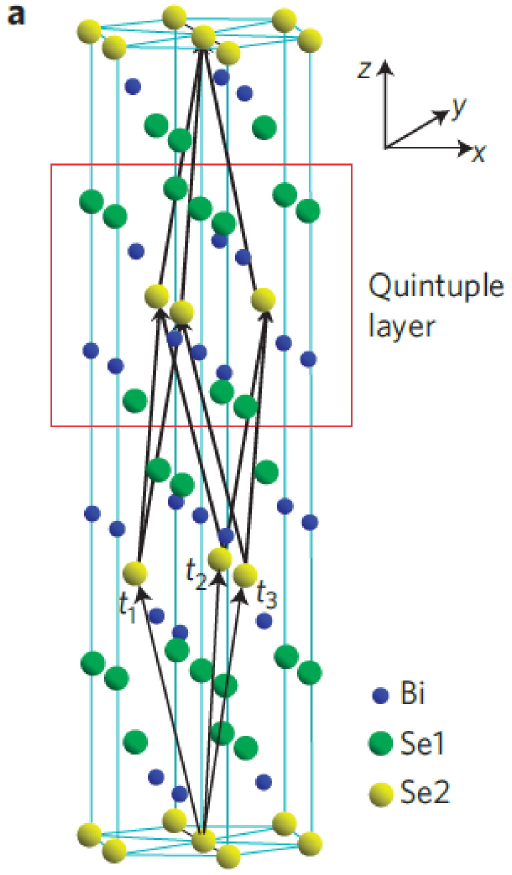

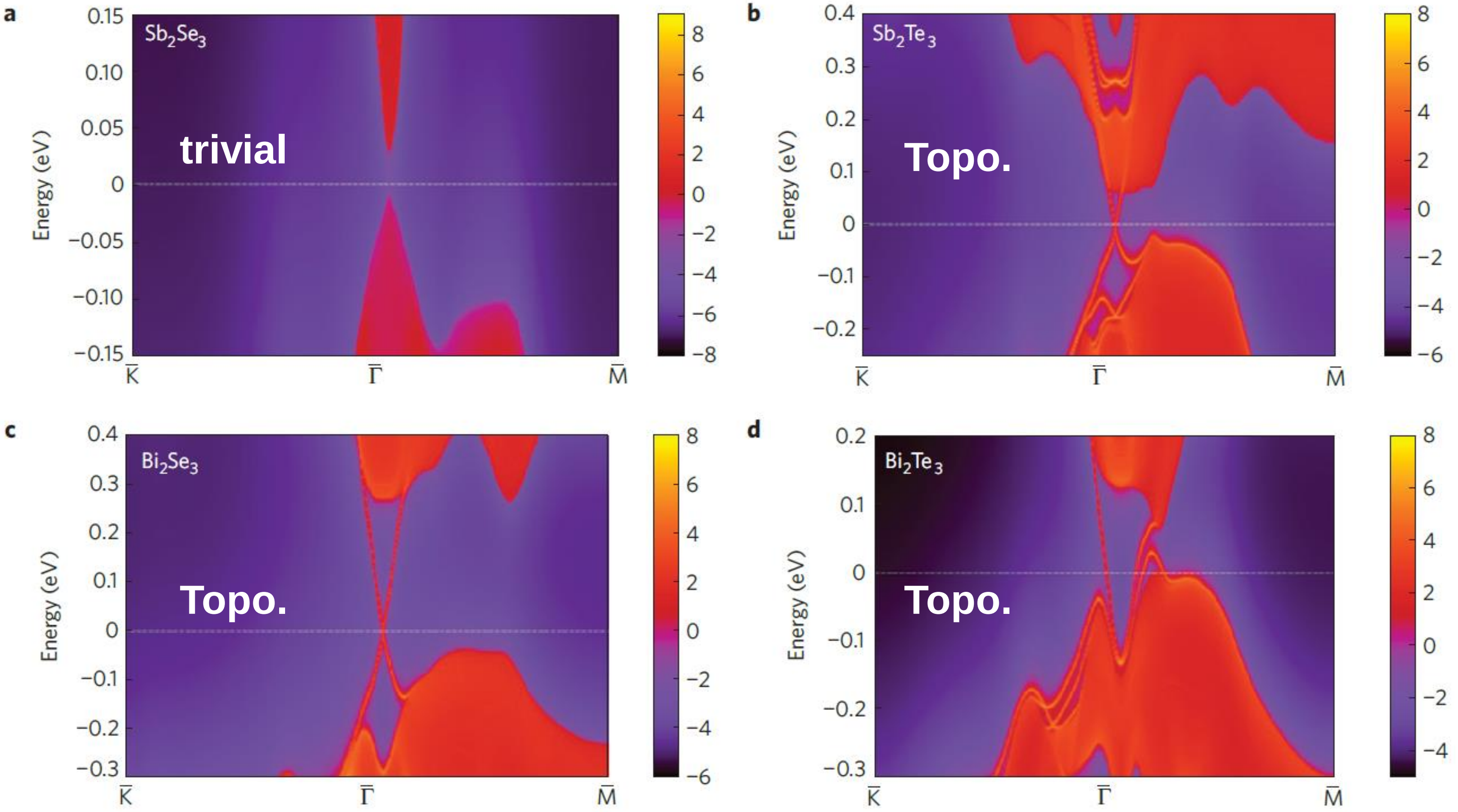

3D - Topological insulators

Ingredient #1

Bi_2Te_2Se

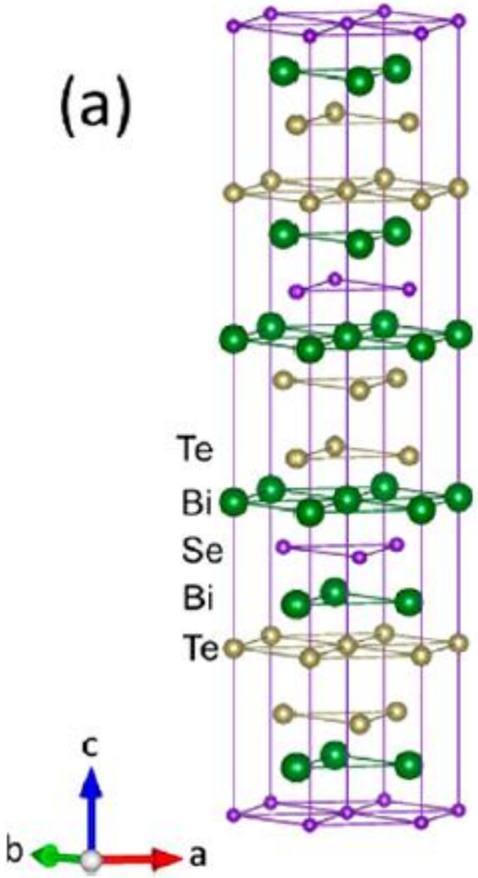

ARPES

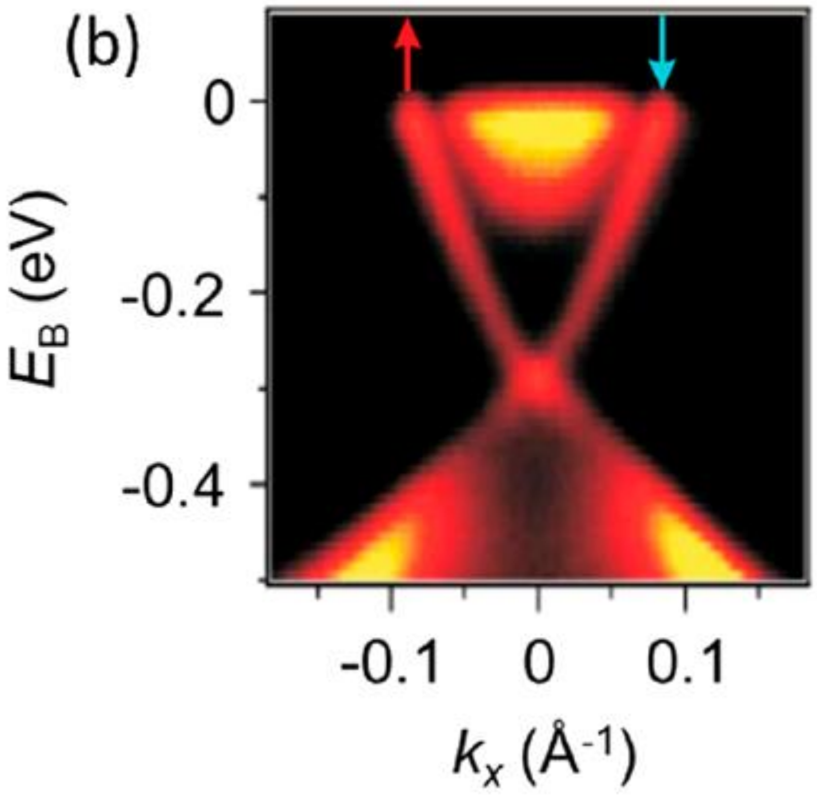

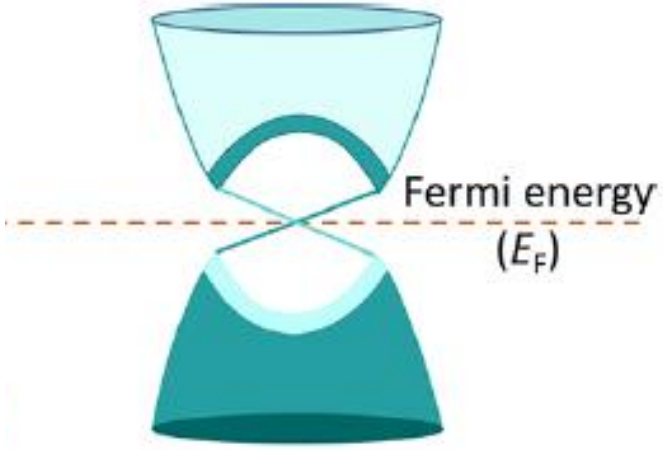

Topological insulator

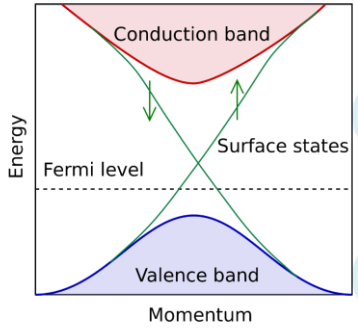

Strong spin-orbit coupling (SOC) with band inversion (at Γ point) generate **topologically protected surface electronic states** crossing the bulk band gap

Kumar et al, "Topological Quantum Materials from the Viewpoint of Chemistry" Chemical Reviews (2021)

3D - Topological insulators

Ingredient #2

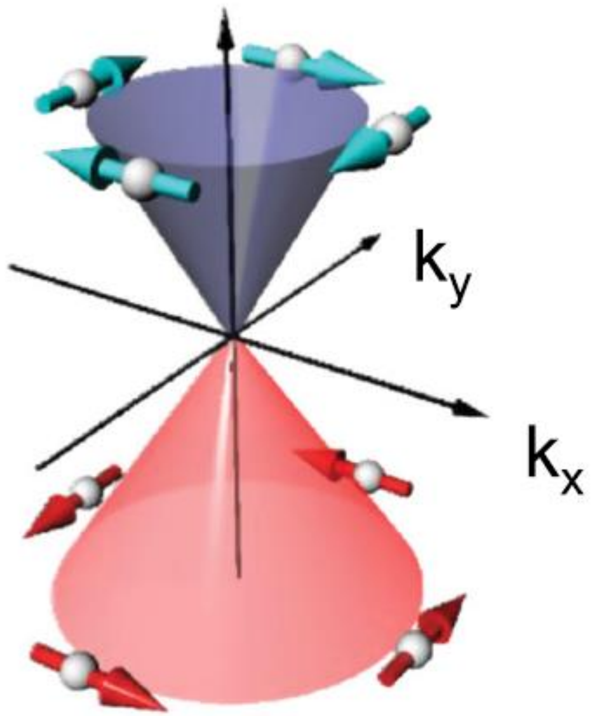

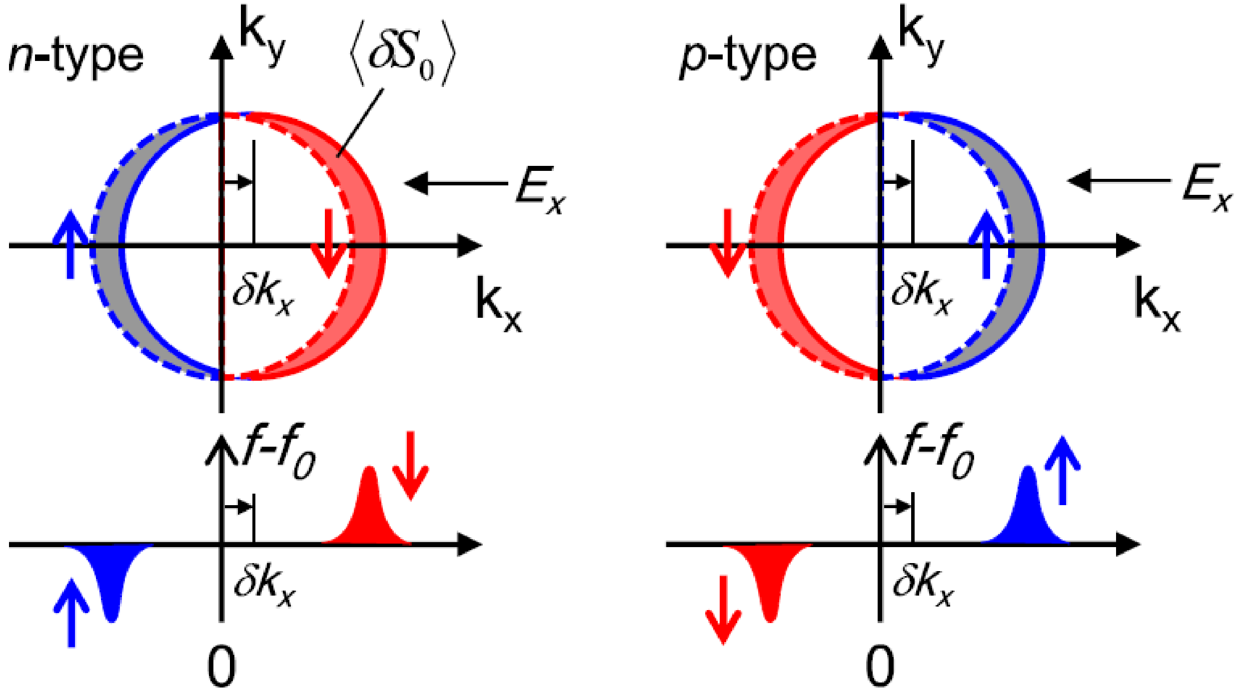

…**topologically-protected surface states show spin-momentum locking**, which prevents backstattering between states of opposite momenta with opposite spins….

W. Han, npj Quantum Materials (2018)

3D - Topological insulators

Fermi level position

$Bi_{1-x}Sb_xTe_3$

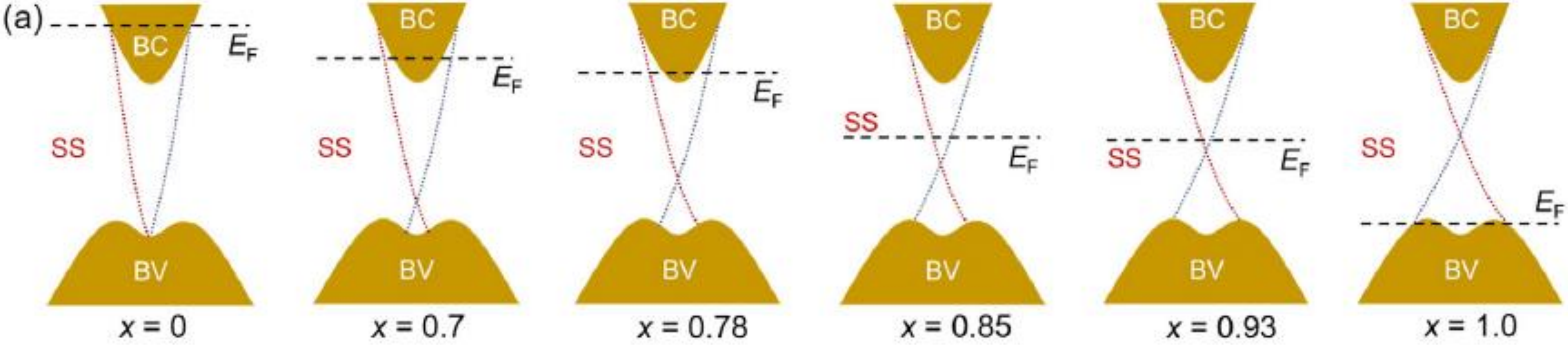

Doping / alloying is a possible way to tune the Fermi level position

Wu et al, "Topological Quantum Materials from the Viewpoint of Chemistry" Phys Rev. Lett. (2019)

Spintronics: from concepts to devices (~10yrs)

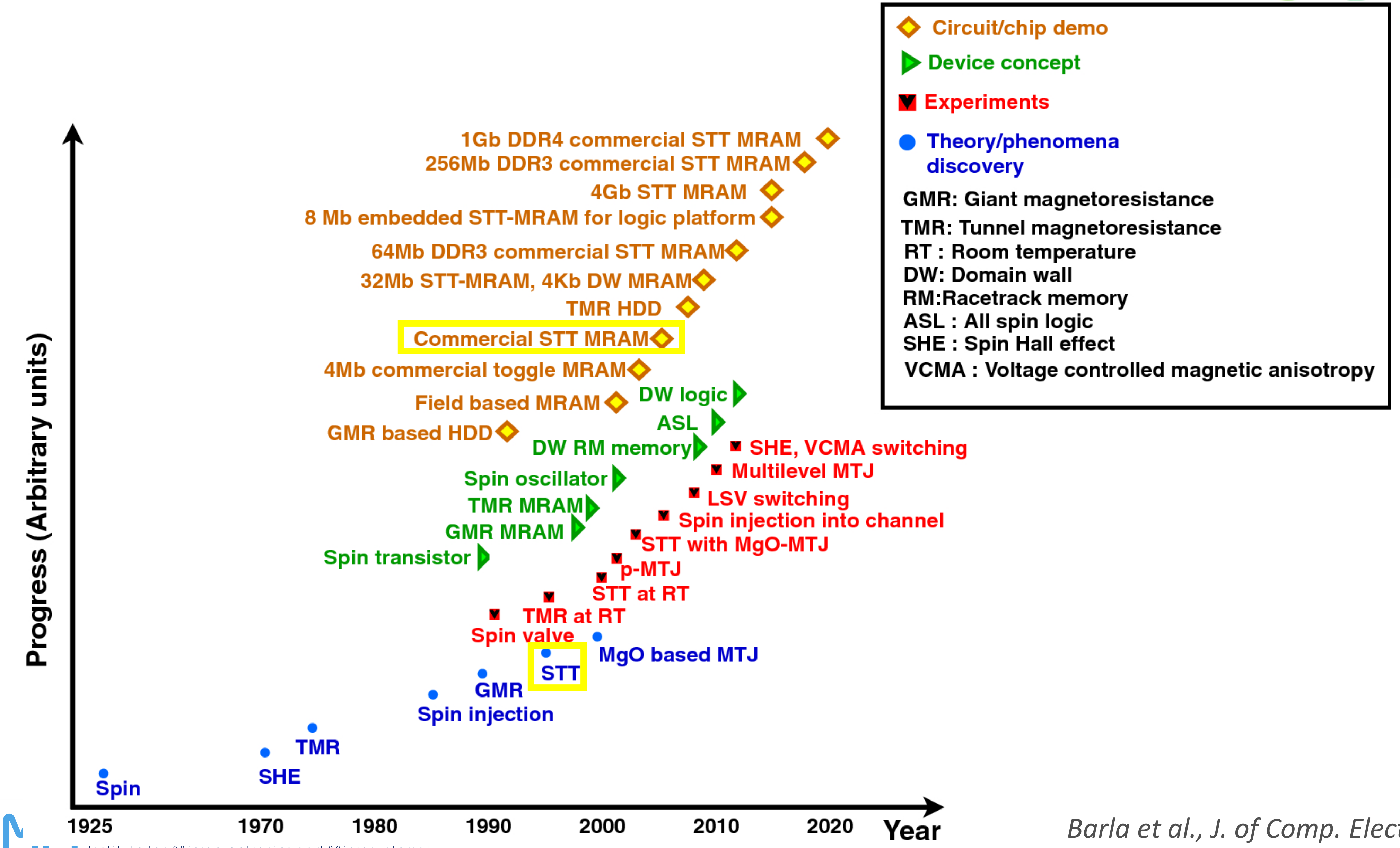

Barla et al., J. of Comp. Electr. 20, 805 (2021)

3D-TI for SOT-MRAM

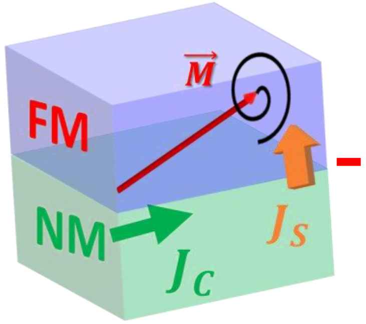

$$\frac{J_S}{J_C}$$

CHARGE-SPIN CONVERSION

Spin Hall Angle
= 1.59 (from SOT)
= 1.09 (from FMR)

$$J_C = 1.4 \times 10^6 \frac{A}{cm^2}$$

ARTICLE
https://doi.org/10.1038/s41467-021-26478-3 OPEN
nature COMMUNICATIONS
Check for updates

2021

Magnetic memory driven by topological insulators

Hao Wu[1,7], Aitian Chen[2,7], Peng Zhang[1,7], Haoran He[1], John Nance[3], Chenyang Guo[4], Julian Sasaki[5], Takanori Shirokura[5], Pham Nam Hai[5,6], Bin Fang[2], Seyed Armin Razavi[1], Kin Wong[1], Yan Wen[2], Yinchang Ma[2], Guoqiang Yu[4], Gregory P. Carman[3], Xiufeng Han[4], Xixiang Zhang[2] & Kang L. Wang[1]

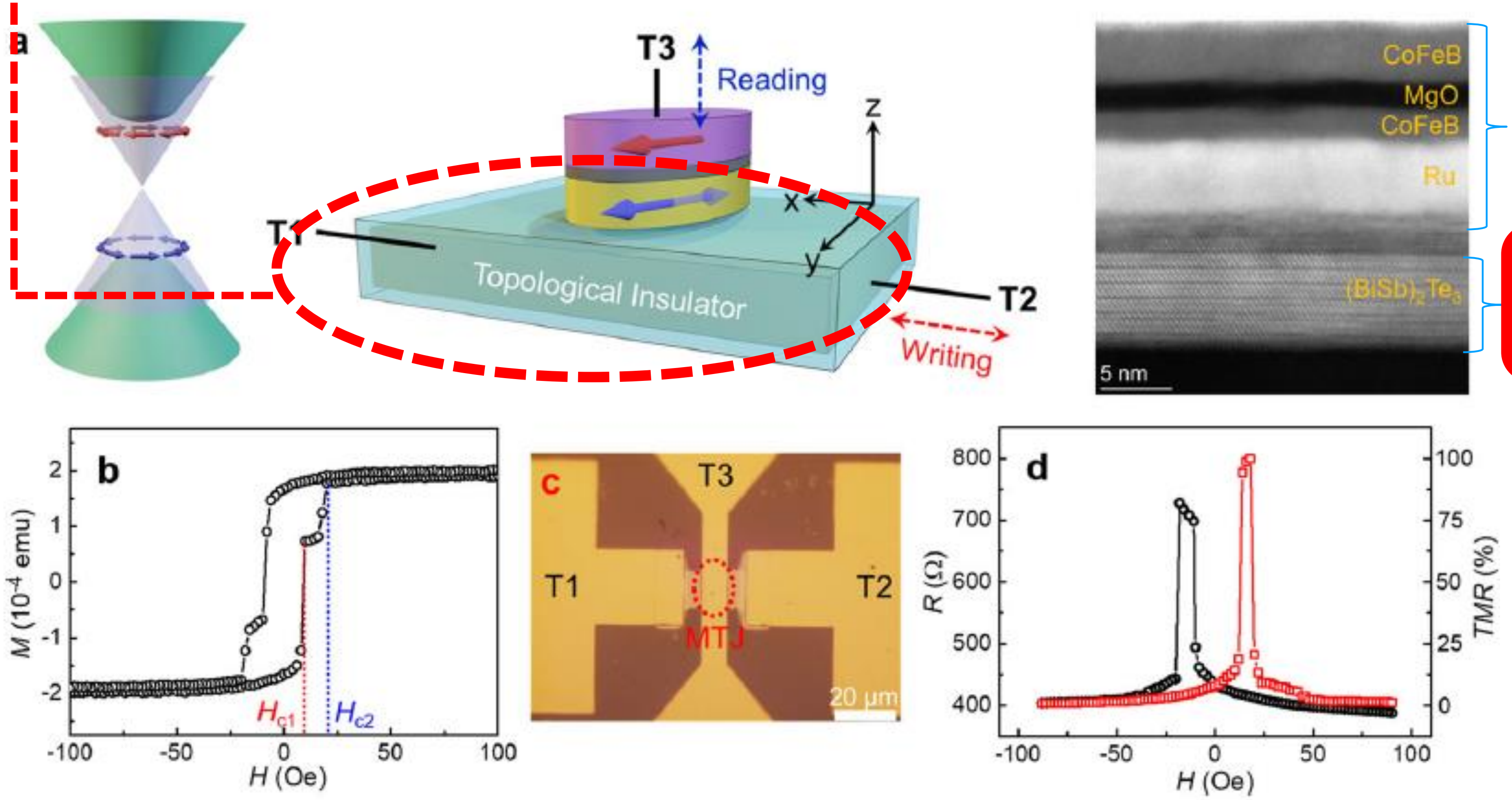

Wu et al, Nat. Comm. (2021)

3D-TI for the MESO

intel 2019

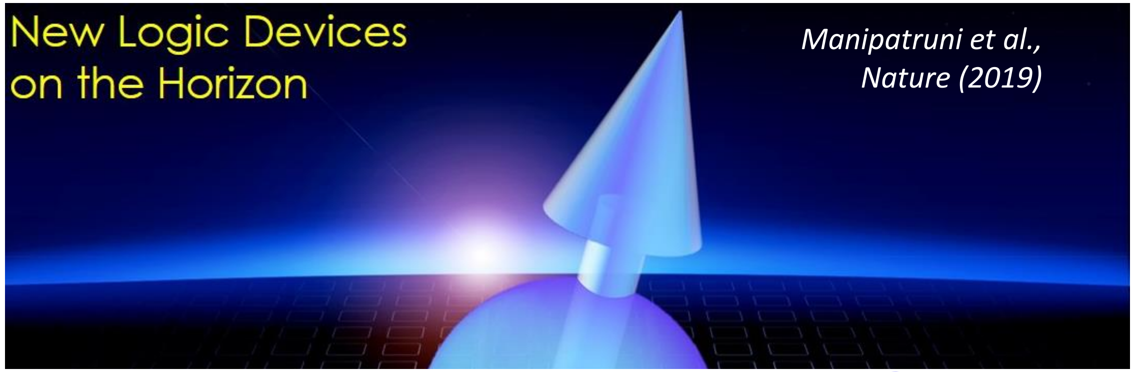

ferromagnet

non-magnetic layer (large SOC)

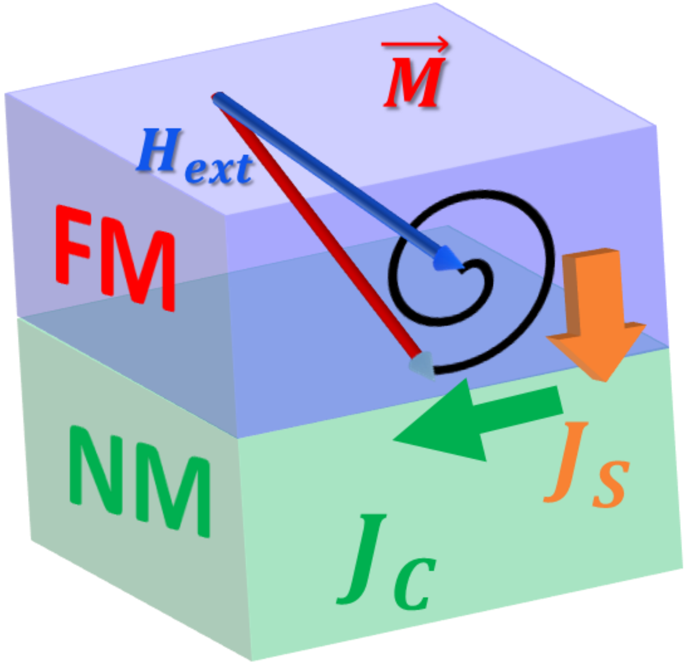

SPIN-CHARGE CONVERSION

ARTICLE

Promise for a 1aJ/switch technology

https://doi.org/10.1038/s41586-018-0770-2

Scalable energy-efficient magnetoelectric spin–orbit logic

Sasikanth Manipatruni[1]*, Dmitri E. Nikonov[1], Chia-Ching Lin[1], Tanay A. Gosavi[1], Huichu Liu[2], Bhagwati Prasad[3], Yen-Lin Huang[3,4], Everton Bonturim[3], Ramamoorthy Ramesh[3,4,5] & Ian A. Young[1]

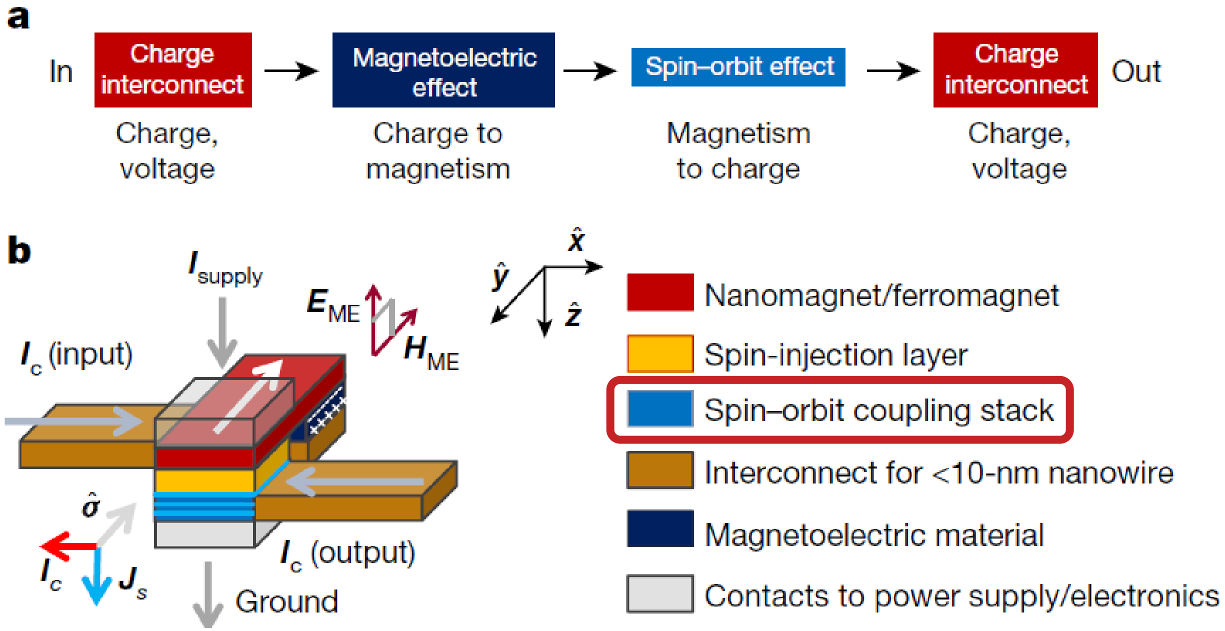

High-SOC and topological oxides	Topological materials and superlattices	Two-dimensional transition-metal dichalcogenides
Bi_2O_3[44], $SrIrO_3$[45], $SrTiO_3/LaAlO_3$[25,36,38]	$Bi_{1.5}Sb_{0.5}Te_{1.7}Se_{1.3}$[24], Bi_2Se_3[34,35], α-Sn[46], BiSb[47]	MoS_2[48], MX_2[49]

Growth methods

To grow TIs over large areas is a necessary prerequisite toward their technology transfer!!

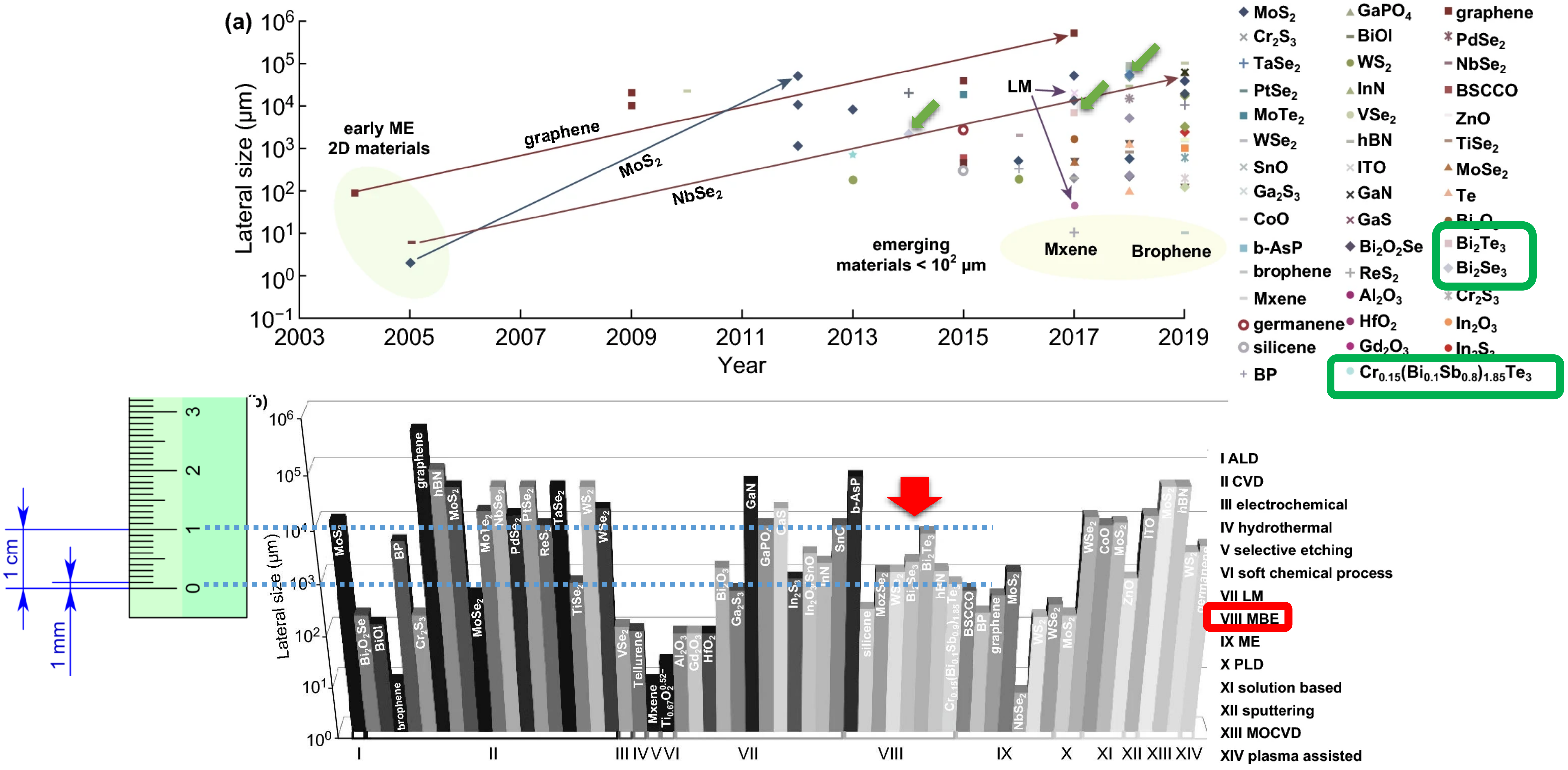

Zavabeti et al., *Nano-Micro Lett.* **12,** 66 (2020)

Summary

- Motivation
  - Topological insulators: intro and applications

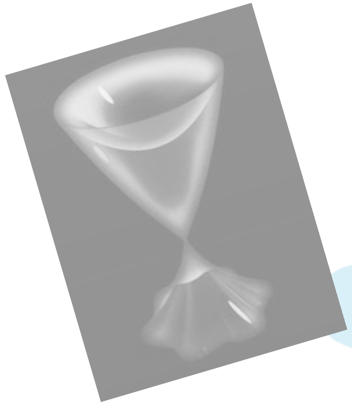

- **MOCVD of topological insulators**
  - Sb_2Te_3, Bi_2Te_3 and Sb_2Te_3/Bi_2Te_3 on large-area Si-based substrates

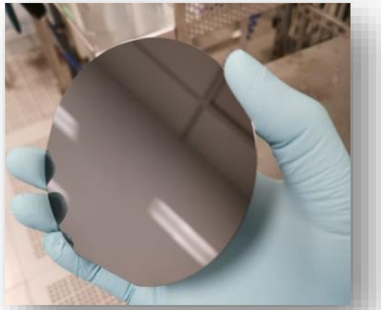

- Spin-charge conversion in MOCVD-TIs
  - The case of Sb_2Te_3 and Sb_2Te_3/Bi_2Te_3

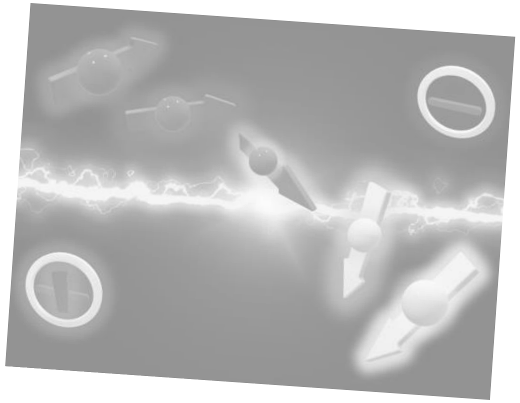

- Conclusions & Outlook

Metal Organic Chemical Vapour Deposition (MOCVD)

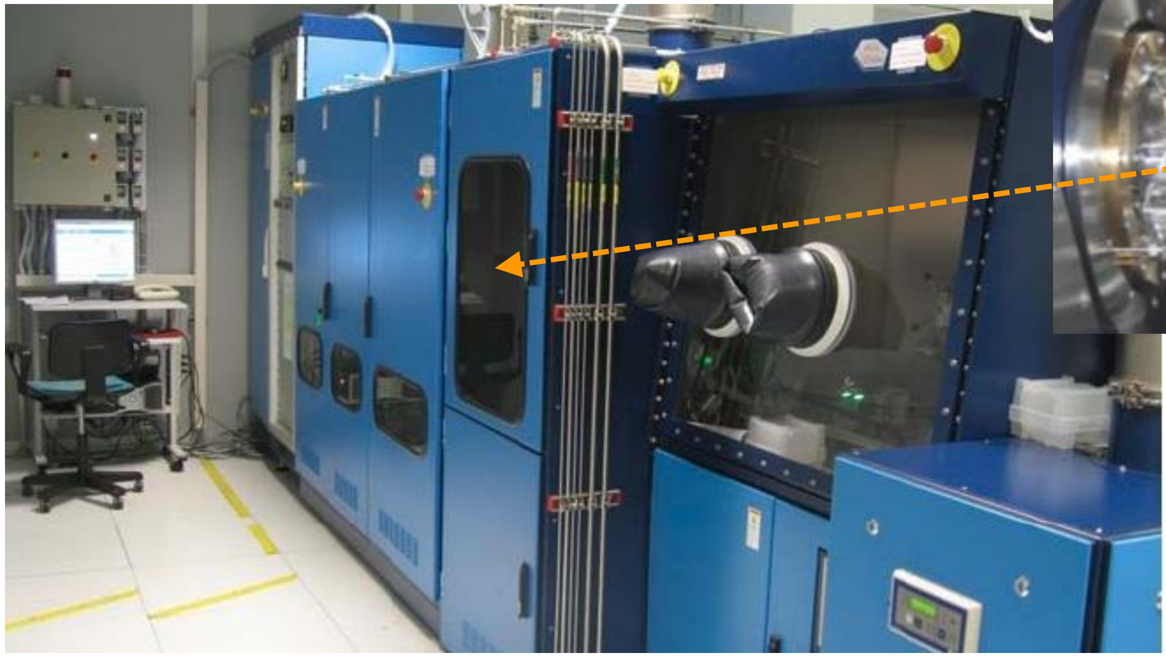

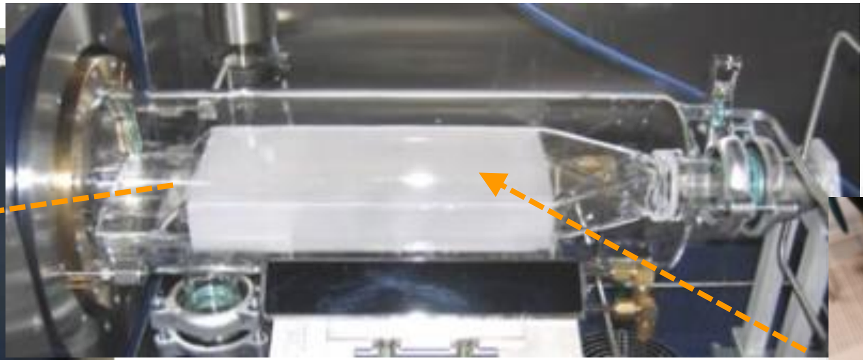

MOCVD is employed at industrial level

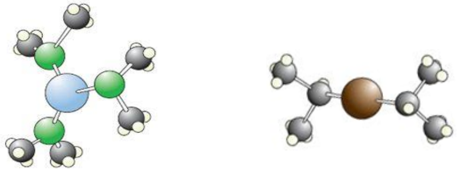

Metalorganic sources

- **Large area (4'')** rotating substrate holder
- N_2 is both carrier and process gas
  No hydride precursors (simple +risk reduction)
- N_2 purity: (<0.1 ppb for H_2O and 0.5 ppb for O_2)

nearly epitaxial Sb_2Te_3 and Bi_2Te_3

Sb Precursor
(TRISDIMETHYLAMINOANTIMONY)
$[N(CH_3)_2]_3$**Sb**

Bi Precursor
(TRIMETHYLBISMUTH)
$(CH_3)_3$**Bi**

Te Precursor
(DIISOPROPYLTELLURIDE)
$(C_3H_7)_2$**Te**

Sb_2Te_3

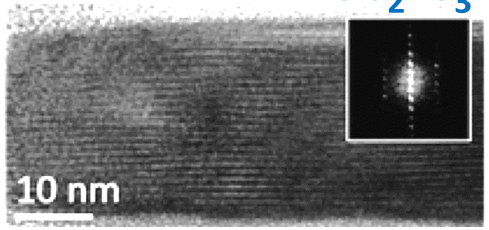

Bi_2Te_3

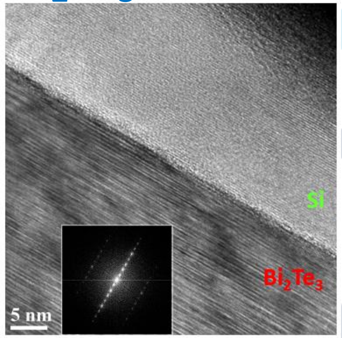

M. Rimoldi et al., RCS Advances (2020)
M. Rimoldi et al., Cryst. Growth & Design (2021)
A. Kumar et al., Cryst. Growth & Design (2021)

Sb_2Te_3 by MOCVD: toward epitaxy

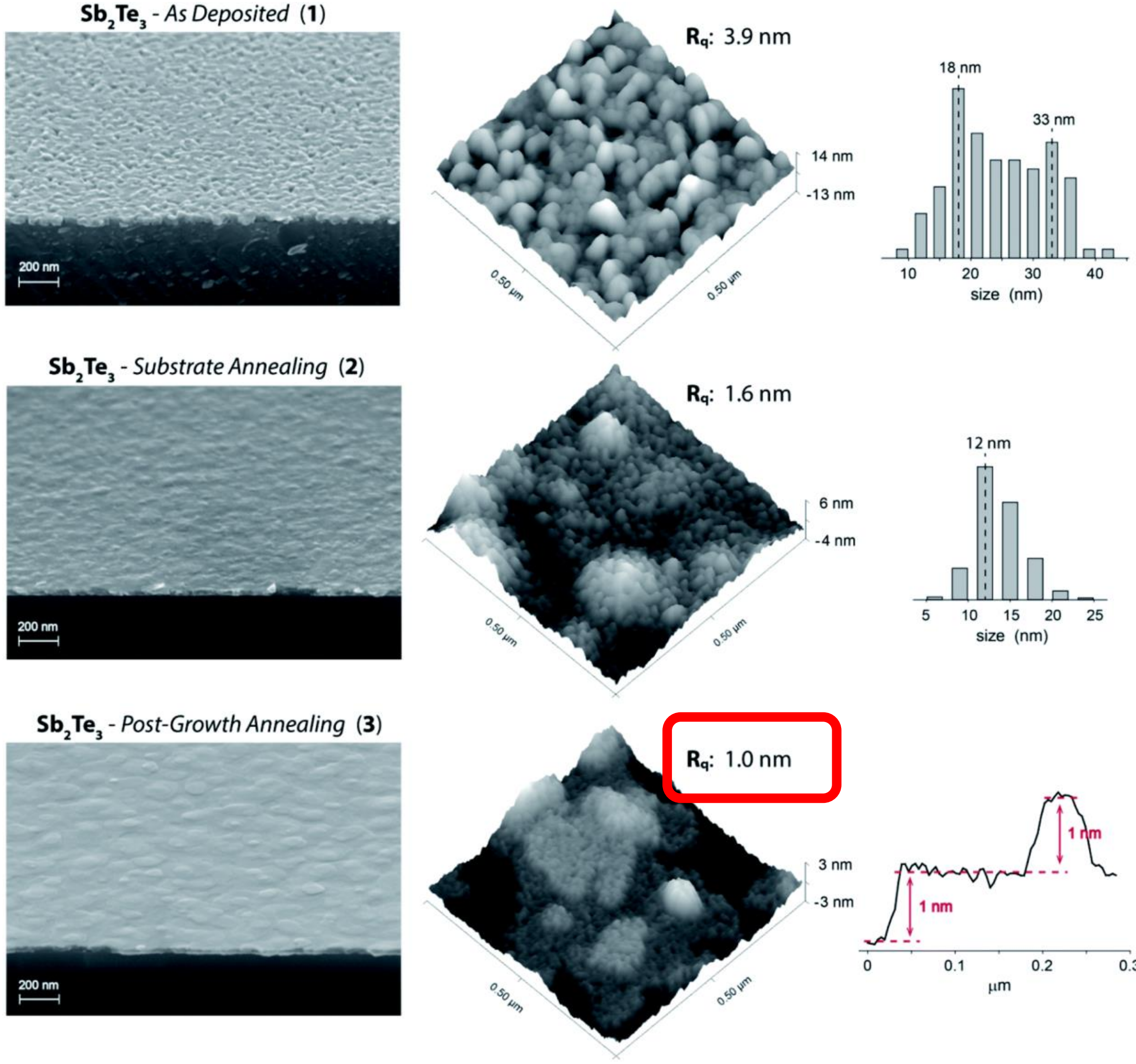

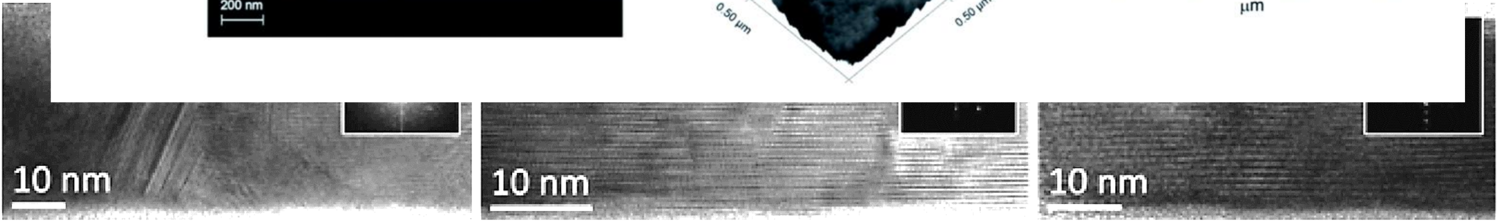

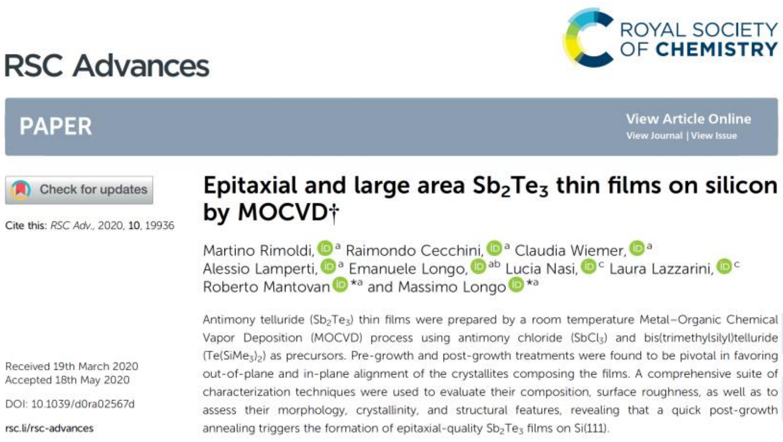
RSC Advances

ROYAL SOCIETY OF CHEMISTRY

PAPER

View Article Online
View Journal | View Issue

Check for updates

Cite this: *RSC Adv.*, 2020, **10**, 19936

Epitaxial and large area Sb_2Te_3 thin films on silicon by MOCVD†

Martino Rimoldi,[a] Raimondo Cecchini,[a] Claudia Wiemer,[a] Alessio Lamperti,[a] Emanuele Longo,[ab] Lucia Nasi,[c] Laura Lazzarini,[c] Roberto Mantovan*[a] and Massimo Longo*[a]

Received 19th March 2020
Accepted 18th May 2020

DOI: 10.1039/d0ra02567d

rsc.li/rsc-advances

Antimony telluride (Sb_2Te_3) thin films were prepared by a room temperature Metal–Organic Chemical Vapor Deposition (MOCVD) process using antimony chloride ($SbCl_3$) and bis(trimethylsilyl)telluride ($Te(SiMe_3)_2$) as precursors. Pre-growth and post-growth treatments were found to be pivotal in favoring out-of-plane and in-plane alignment of the crystallites composing the films. A comprehensive suite of characterization techniques were used to evaluate their composition, surface roughness, as well as to assess their morphology, crystallinity, and structural features, revealing that a quick post-growth annealing triggers the formation of epitaxial-quality Sb_2Te_3 films on Si(111).

From granular to nearly epitaxial Sb_2Te_3 thin films through appropriate thermal processing

Si(111) substrates

Sb_2Te_3 surface roughness strongly reduced

→ Possible integration of layers on top

MOCVD of Bi_2Te_3

Bragg-Brentano analysis

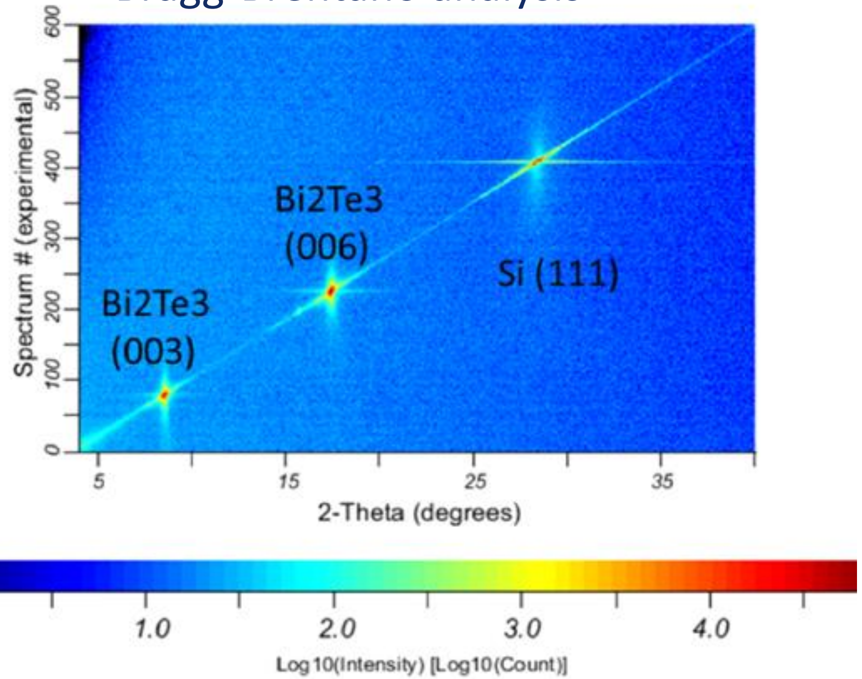

- **Rombohedral** crystalline structure (R-3m)
- Bi_2Te_3 shows lower mosaicity (less broadening) than Sb_2Te_3

pubs.acs.org/crystal Article

Large-Area MOVPE Growth of Topological Insulator Bi_2Te_3 Epitaxial Layers on i-Si(111)

Arun Kumar, Raimondo Cecchini, Lorenzo Locatelli, Claudia Wiemer, Christian Martella, Lucia Nasi, Laura Lazzarini, Roberto Mantovan,* and Massimo Longo*

CRYSTAL GROWTH & DESIGN

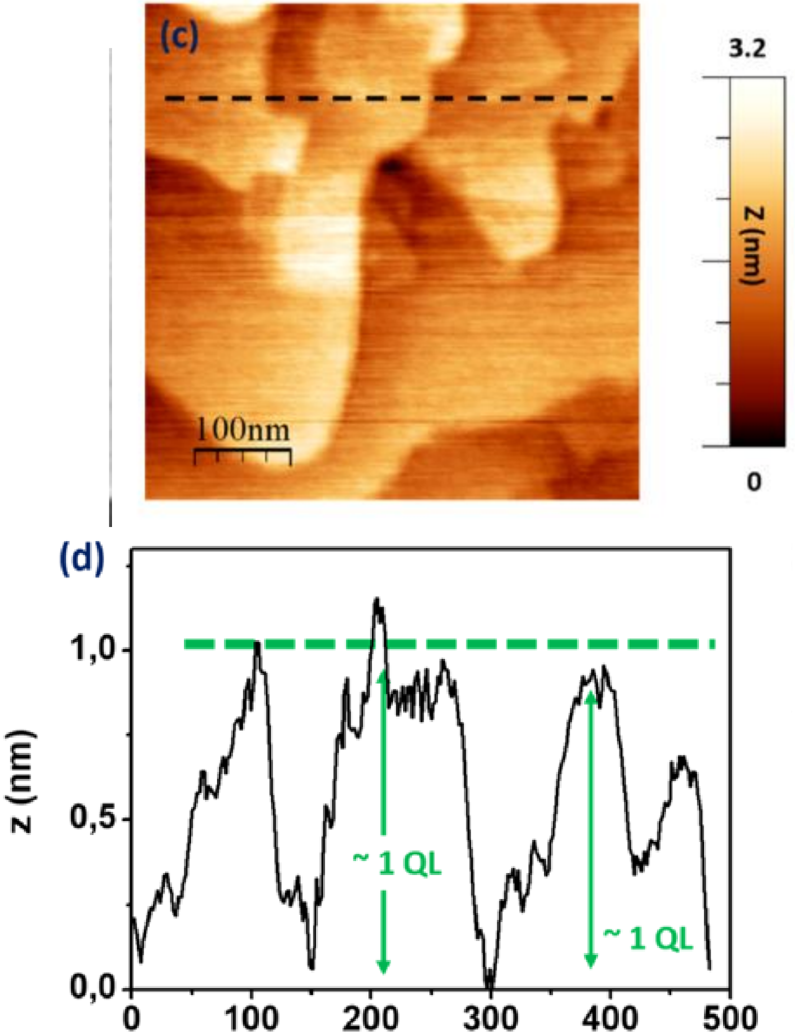

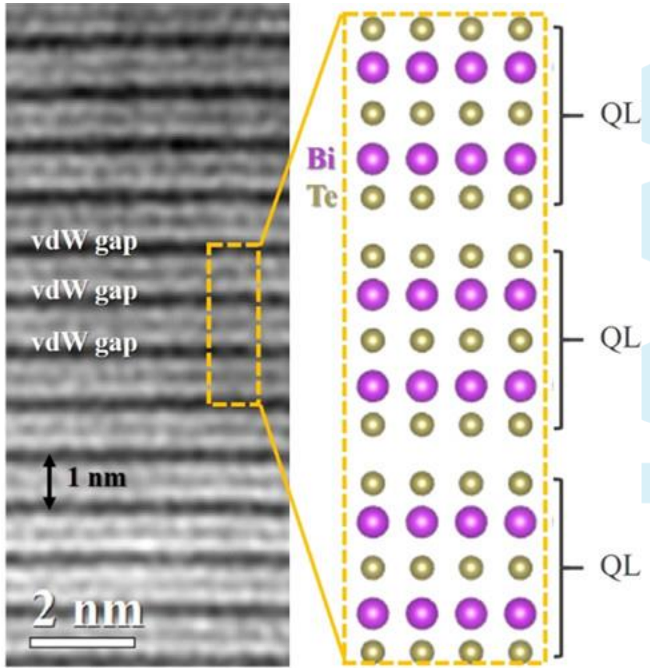

- **Within platelets rms is ~0.5 nm**
- **Steps of 1QL (~1 nm)** every few hundreads of nm

Characterization of topology: magnetotransport

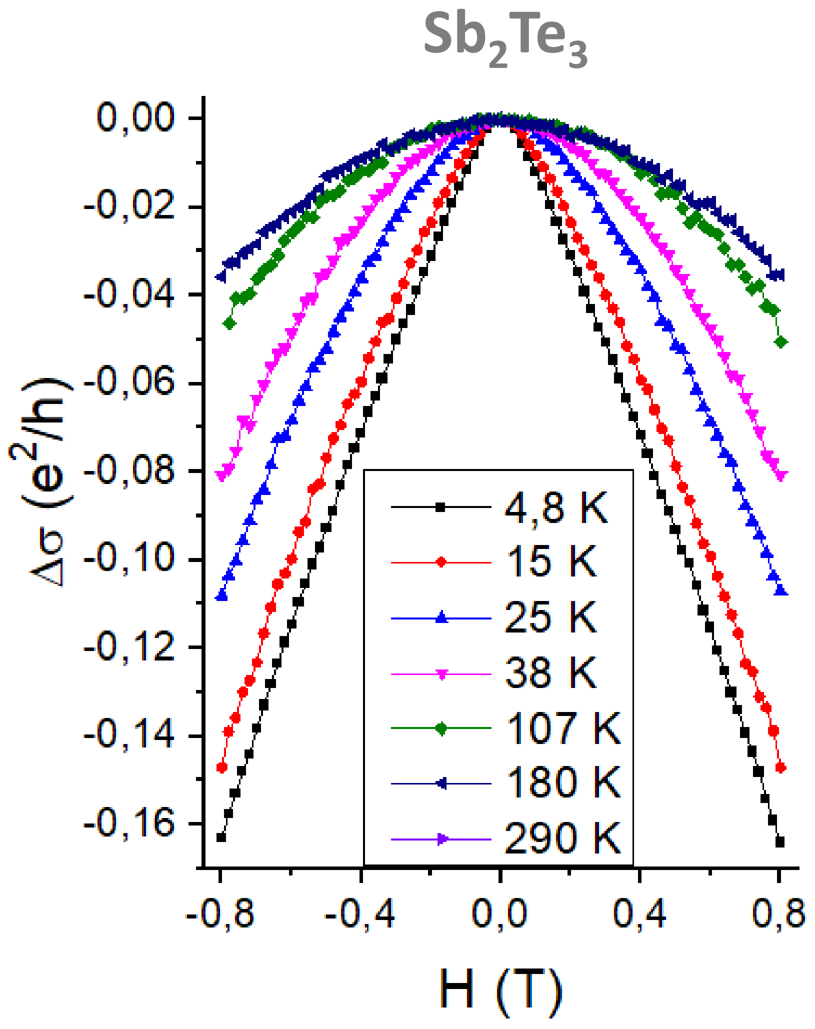

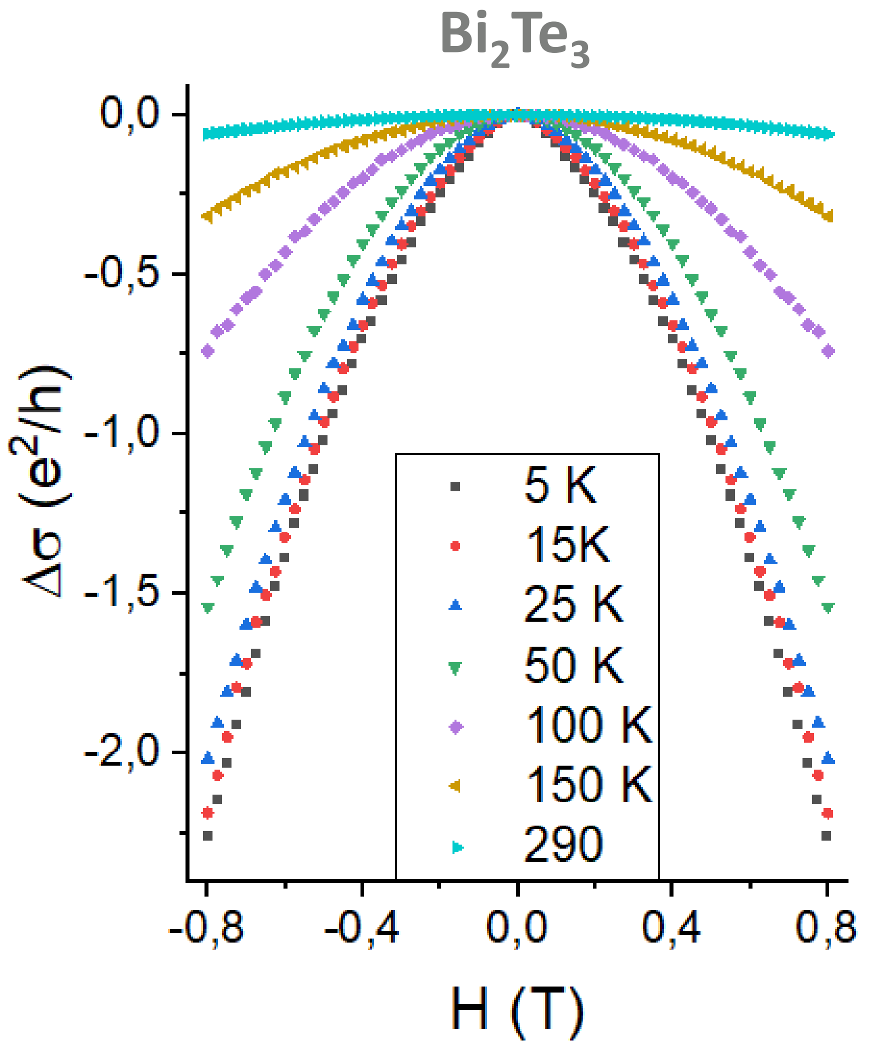

Weak Antilocalization (WAL) emerges at low T in the MC curves

L. Locatelli et al.,Sci. Rep. (2022)

WAL interpreted within the HLN model

$$\Delta\sigma_s = -\alpha \frac{e^2}{\pi h} \left(\Psi\left(\frac{1}{2} + \frac{h}{8\pi e l_\phi^2 B}\right) - ln\left(\frac{h}{8\pi e l_\phi^2 B}\right)\right)$$

Hikami-Larkin-Nagaoka (HLN) model
(*Lorentzian part removed)*

- **α : Proportional to the number of 2D conductive channel (= -0.5 for one channel and = -1.0 for two channels)**
- **l_ϕ: Spin coherence length**

@5K

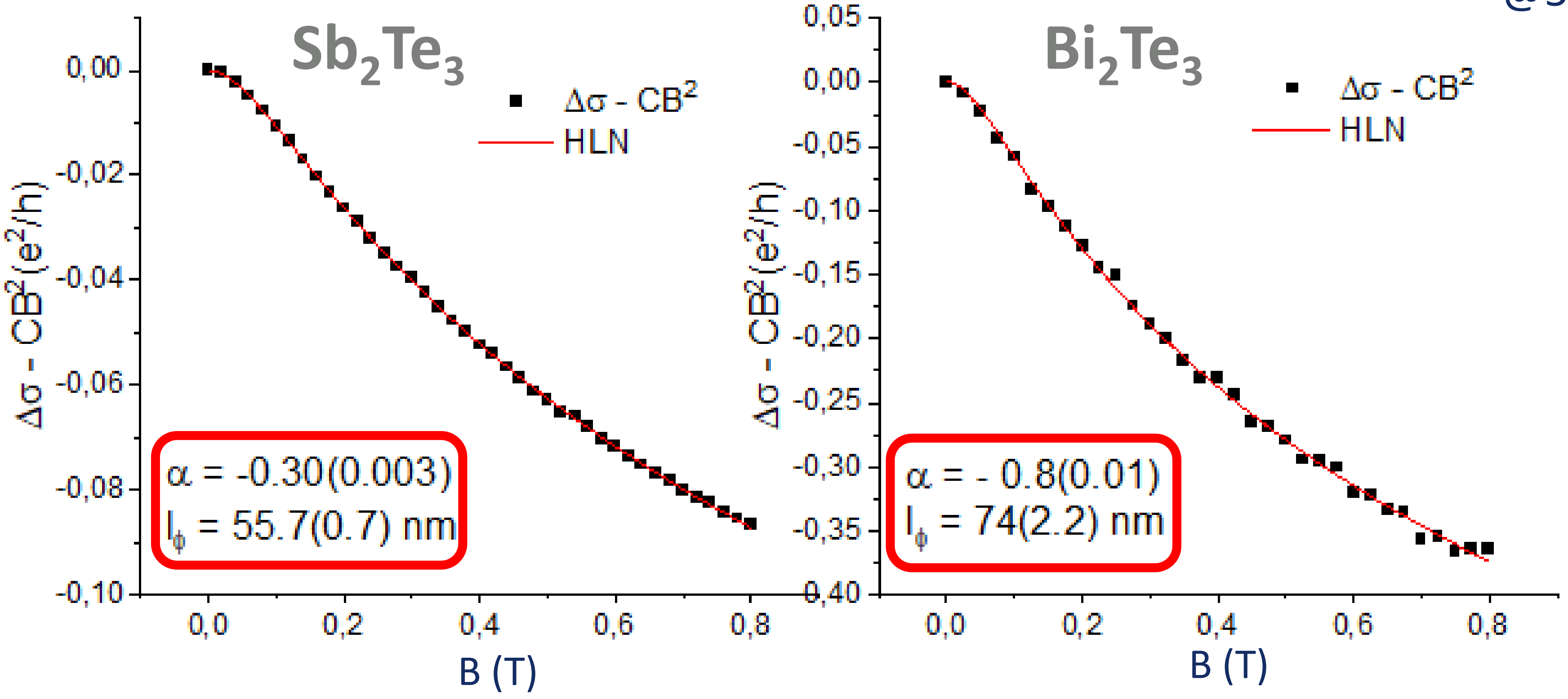

→ **2D-type of conduction** demonstrated

L. Locatelli et al.,Sci. Rep. (2022)

ARPES of our MOCVD 3D-TIs

DEMOKRITOS
NATIONAL CENTRE FOR SCIENTIFIC RESEARCH

- Energy map

Sb_2Te_3

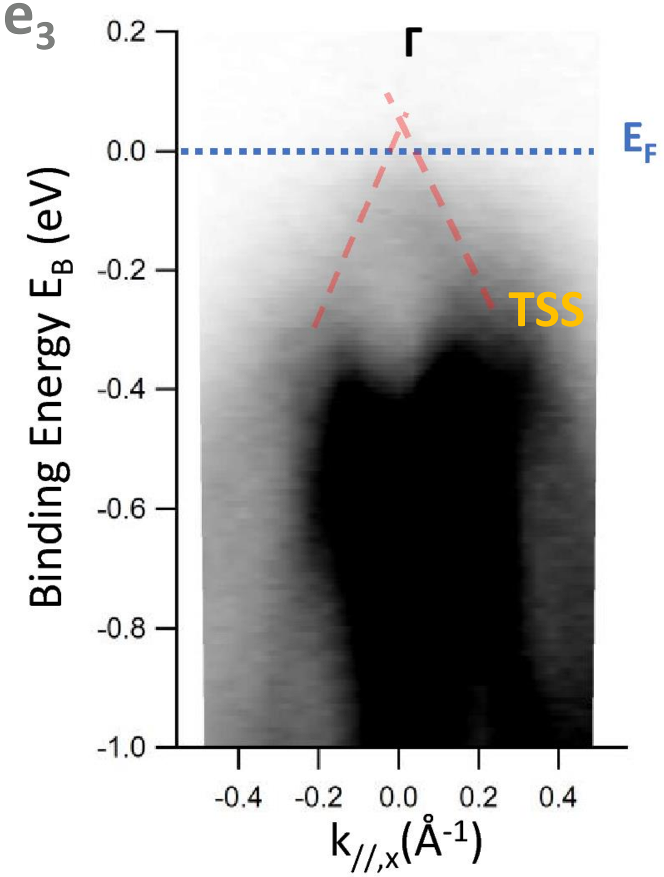

Bi_2Te_3

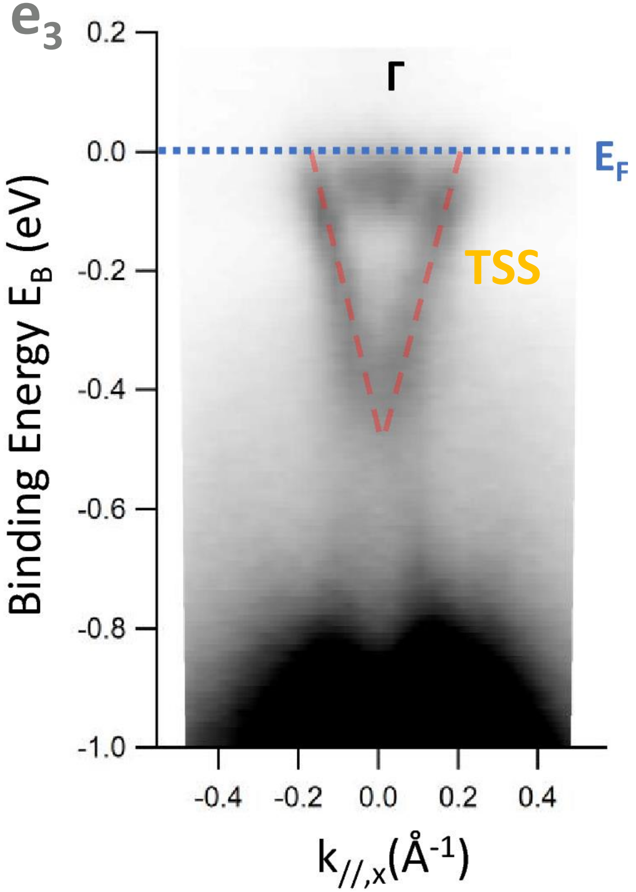

- **Dirac Point only 0.1 eV above E_F**
- **Dirac Point 0.5 eV below E_F**

L. Locatelli et al.,Sci. Rep. (2022)

ARPES of our MOCVD 3D-TIs

DEMOKRITOS
NATIONAL CENTRE FOR SCIENTIFIC RESEARCH

- Polar map at constant energy

Sb_2Te_3
- **only TSS contribute to the Fermi Energy**
- no sign of trigonal-bulk contribution)

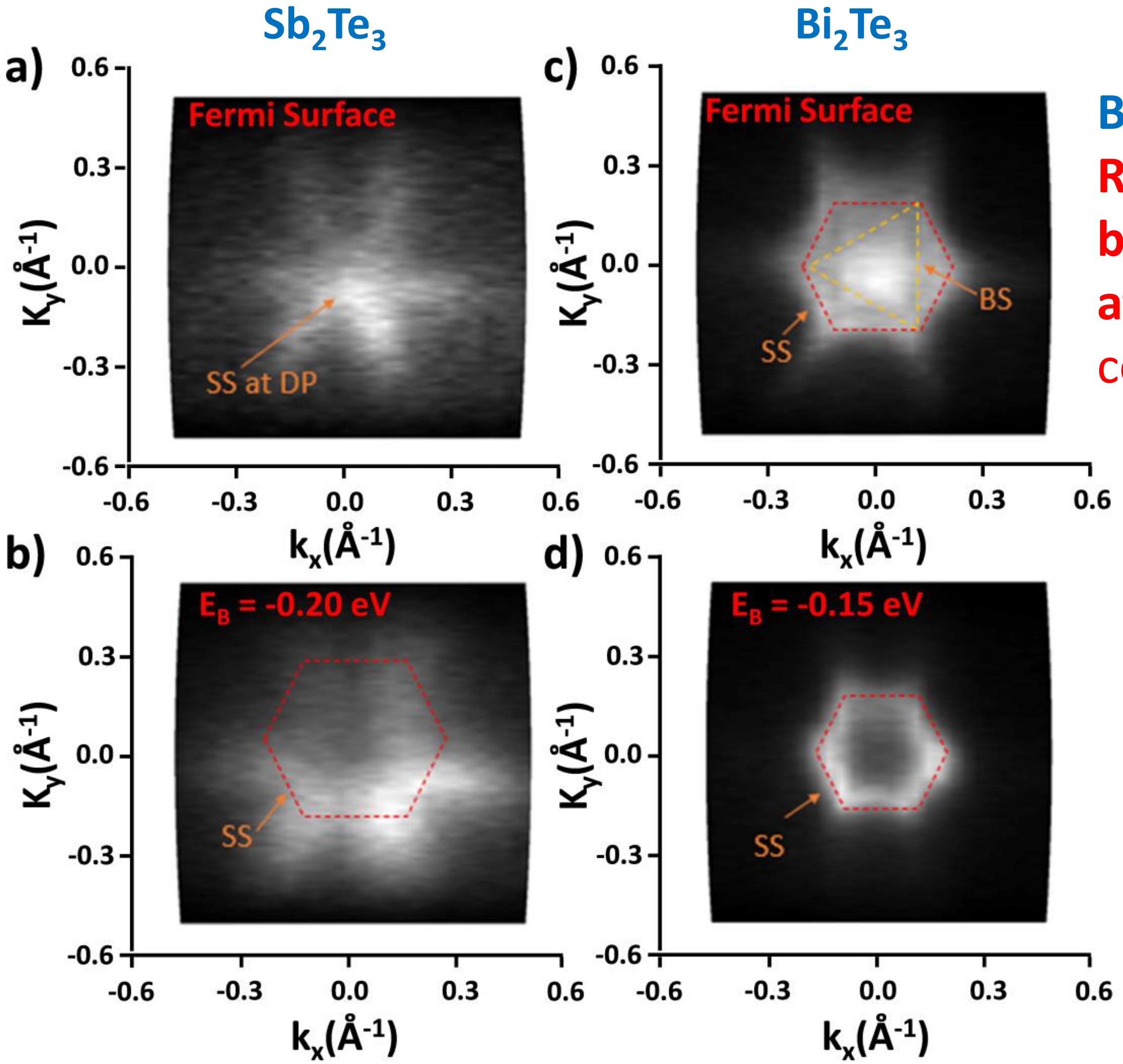

Bi_2Te_3
Relevant (trigonal) bulk contribution at the Fermi level, coexisting with TSS

Sb_2Te_3 is our 1st choice to be used in devices

Bi_2Te_3 → need to be optimized

L. Locatelli et al.,Sci. Rep. (2022)

MOCVD of Sb_2Te_3/Bi_2Te_3

ARPES

DEMOKRITOS
NATIONAL CENTRE FOR SCIENTIFIC RESEARCH

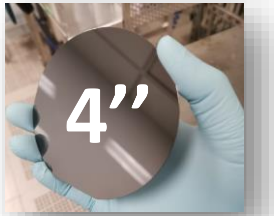

- MOCVD growth of **30 nm** epitaxial Sb_2Te_3
- *In situ* over-growth of **90 nm** Bi_2Te_3 at 350°C

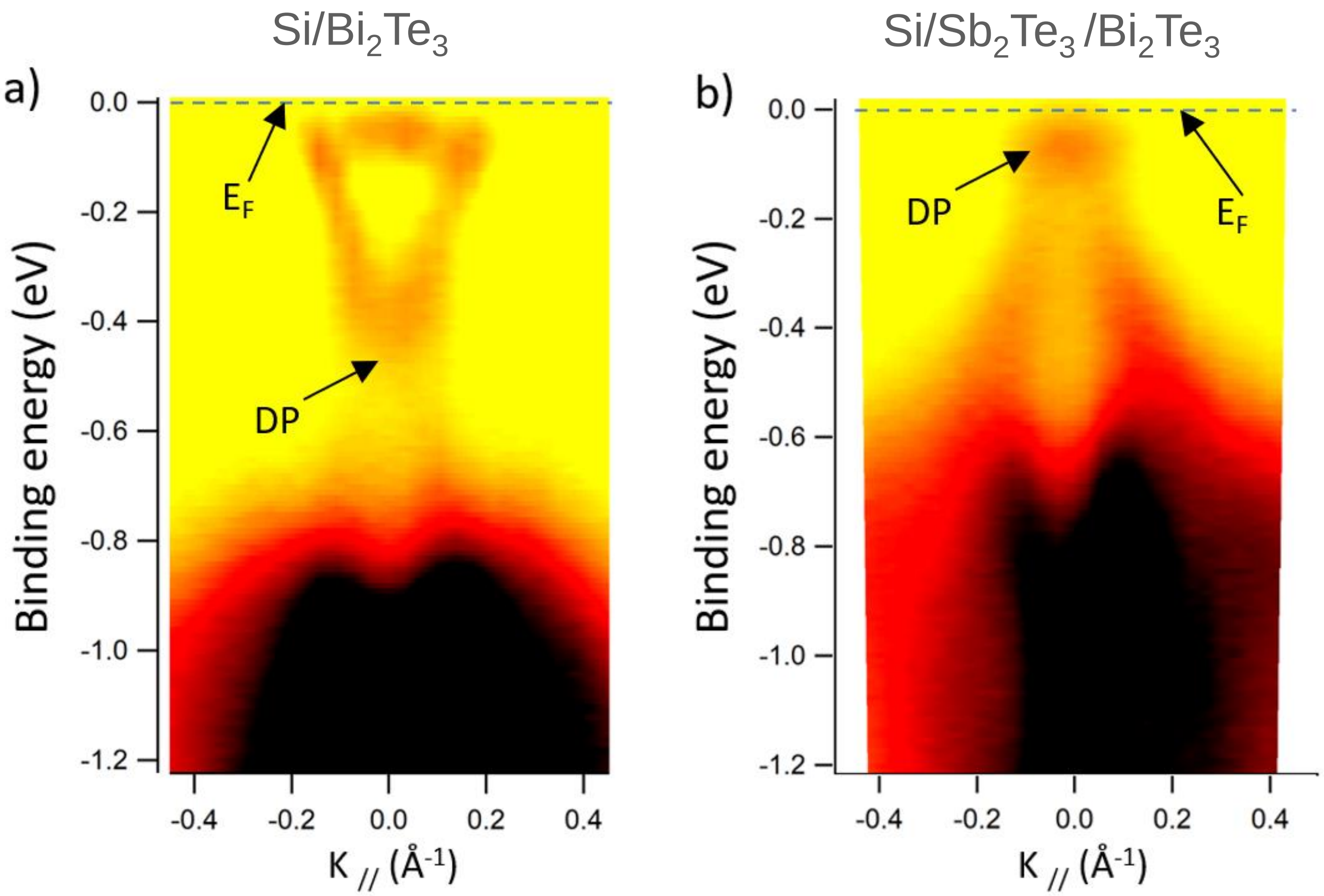

Fermi level of Bi_2Te_3 rigidly shifted toward DP

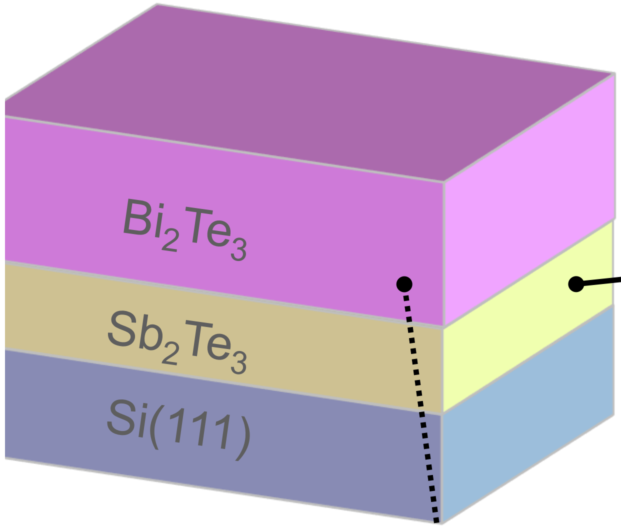

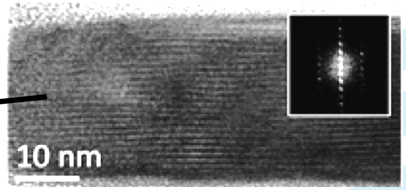

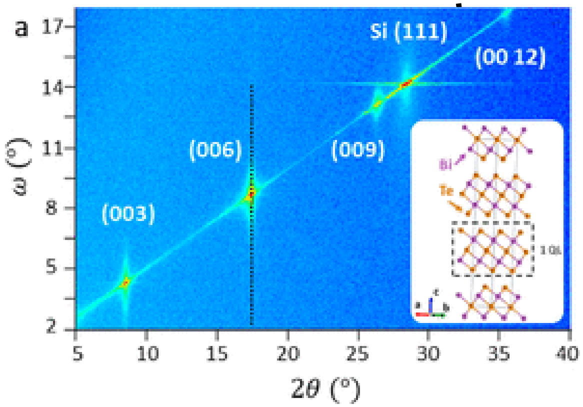

Bragg-Brentano XRD map highlighting the *00l* peaks of Bi_2Te_3

E. Longo. L. Locatelli et al., ACS Appl. Mater. Interfaces (2023)

MOCVD of Sb_2Te_3/Bi_2Te_3

ARPES

DEMOKRITOS
NATIONAL CENTRE FOR SCIENTIFIC RESEARCH

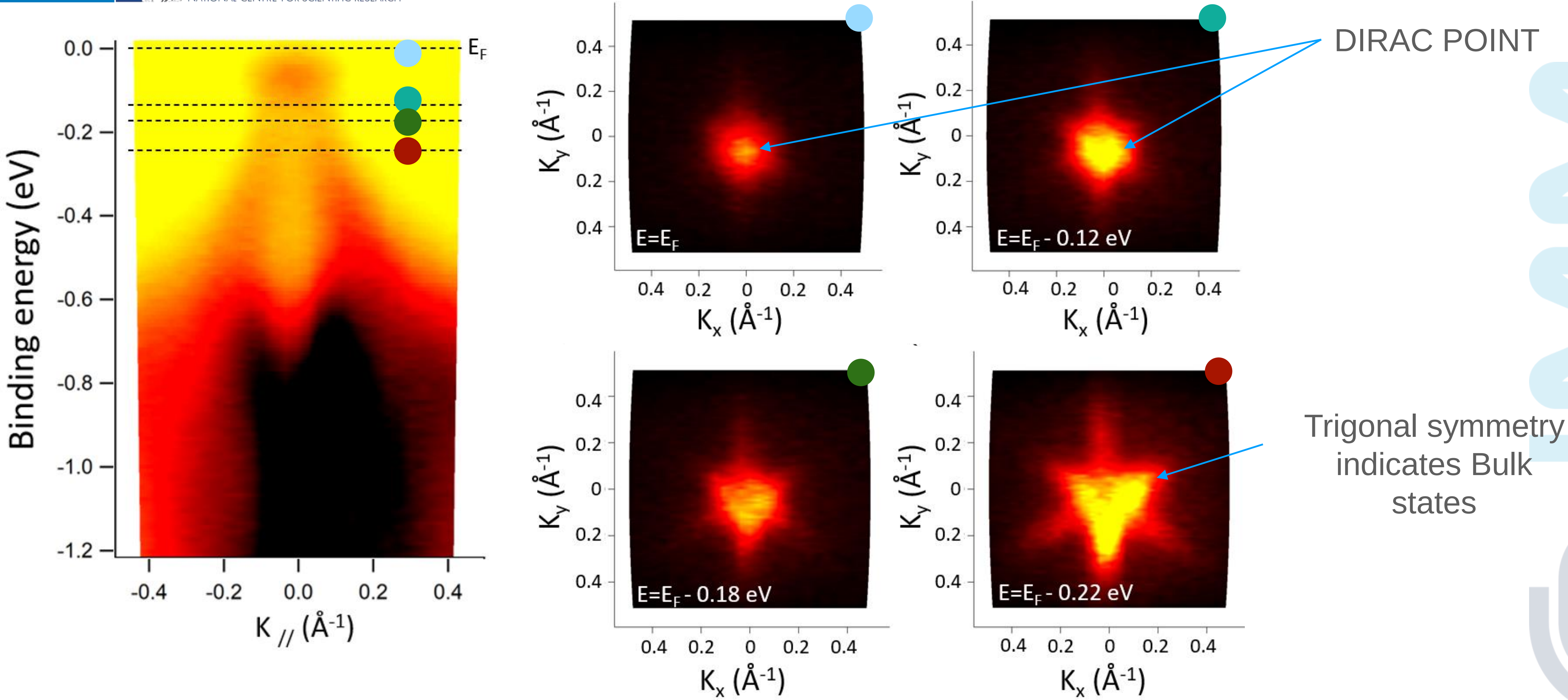

Only hexagonal TSS at E_F

E. Longo. L. Locatelli et al., ACS Appl. Mater. Interfaces (2023)

Summary

- ○ **Motivation**
  - • Topological insulators: intro and applications

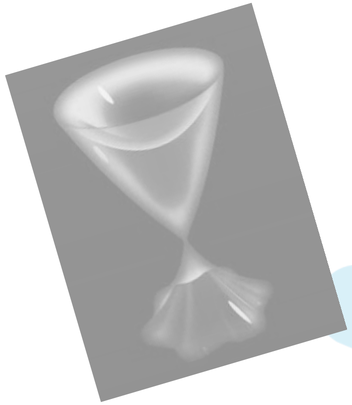

- ○ **MOCVD of topological insulators**
  - • Sb_2Te_3, Bi_2Te_3 and Sb_2Te_3/Bi_2Te_3 on large-area Si-based substrates

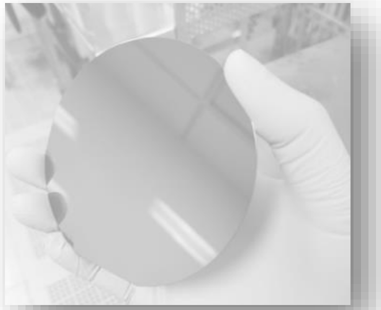

- ○ **Spin-charge conversion in MOCVD-TIs**
  - • The case of Sb_2Te_3 and Sb_2Te_3/Bi_2Te_3

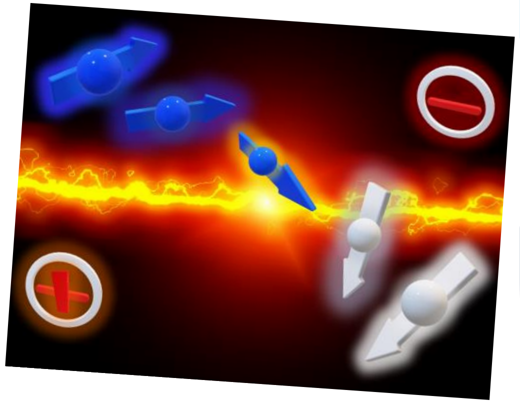

- ○ **Conclusions & Outlook**

Spin pumping ferromagnetic resonance (SP-FMR)

at room T

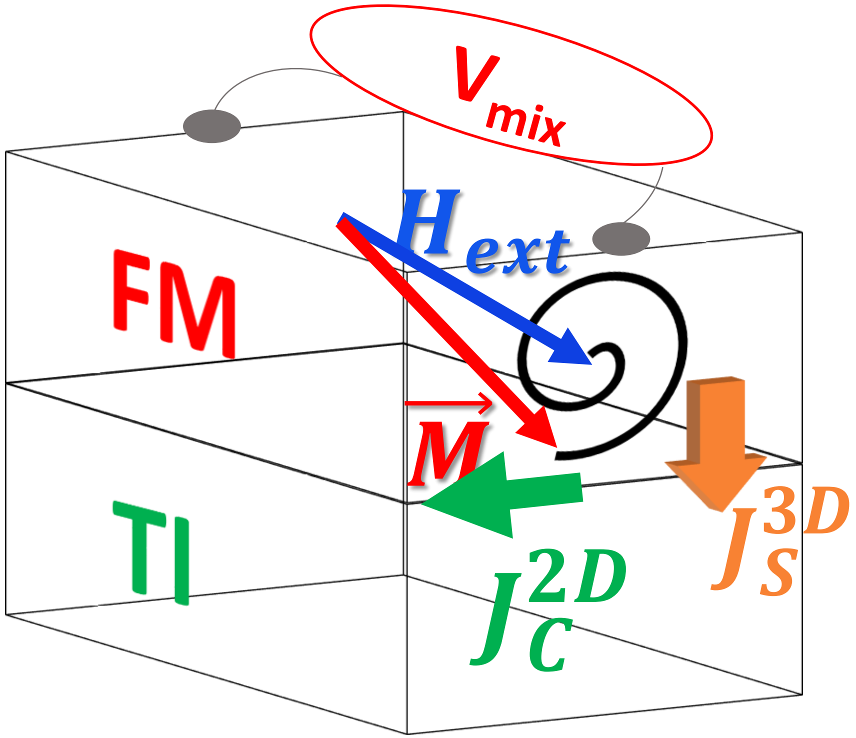

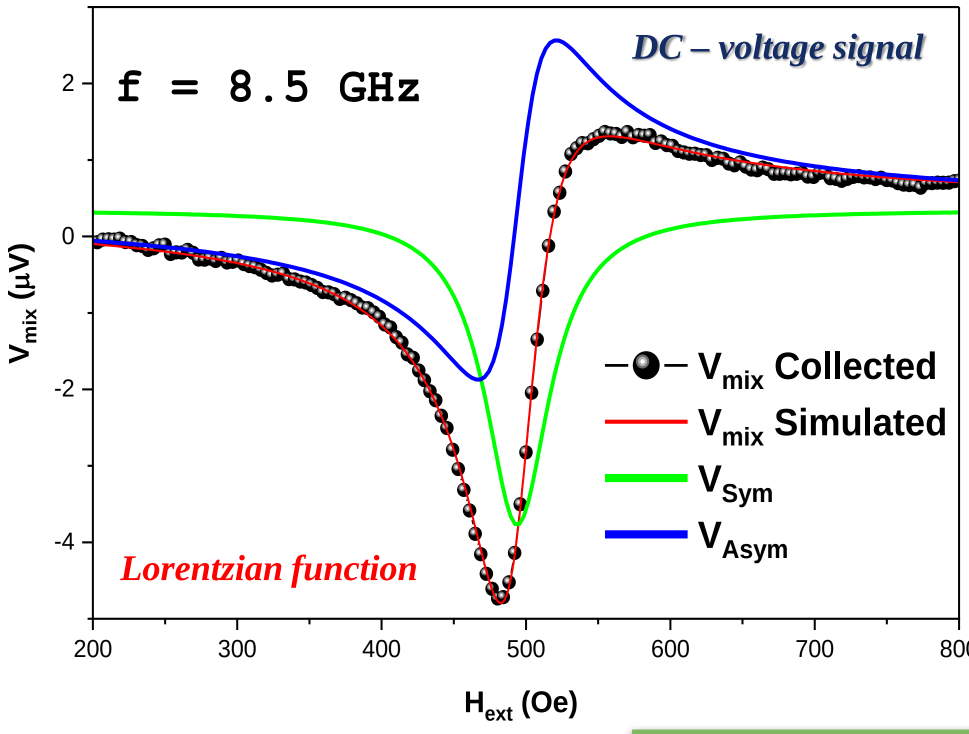

$$V_{mix} = V_{Sym}\frac{\Delta H^2}{\Delta H^2 + (H - H_{res})^2} + V_{Asym}\frac{\Delta H(H - H_{res})}{\Delta H^2 + (H - H_{res})^2}$$

Spin Pumping **Rectification effects**

SPIN PUMPING IS ELECTRICALLY DETECTED (V_{mix}) AT RESONANCE CONDITION

Simple Spin-Charge converters

Following MOCVD of Sb_2Te_3 samples are quickly transferred to e-beam evaporator

e-beam evaporator:
GROWTH of Co (or Fe) with Au interlayer

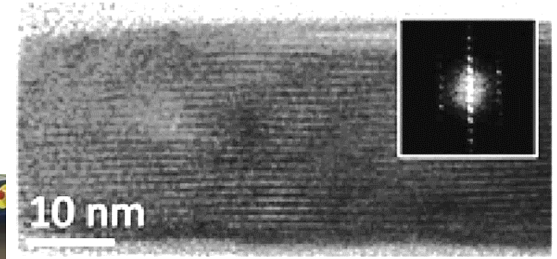

MOCVD of ***large area Sb_2Te_3 topological insulators on Si(111)***

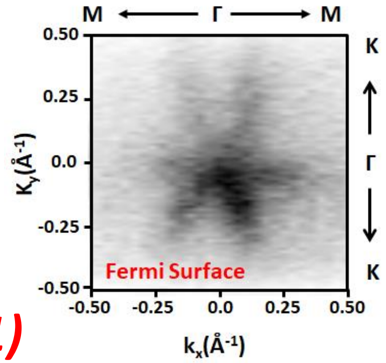

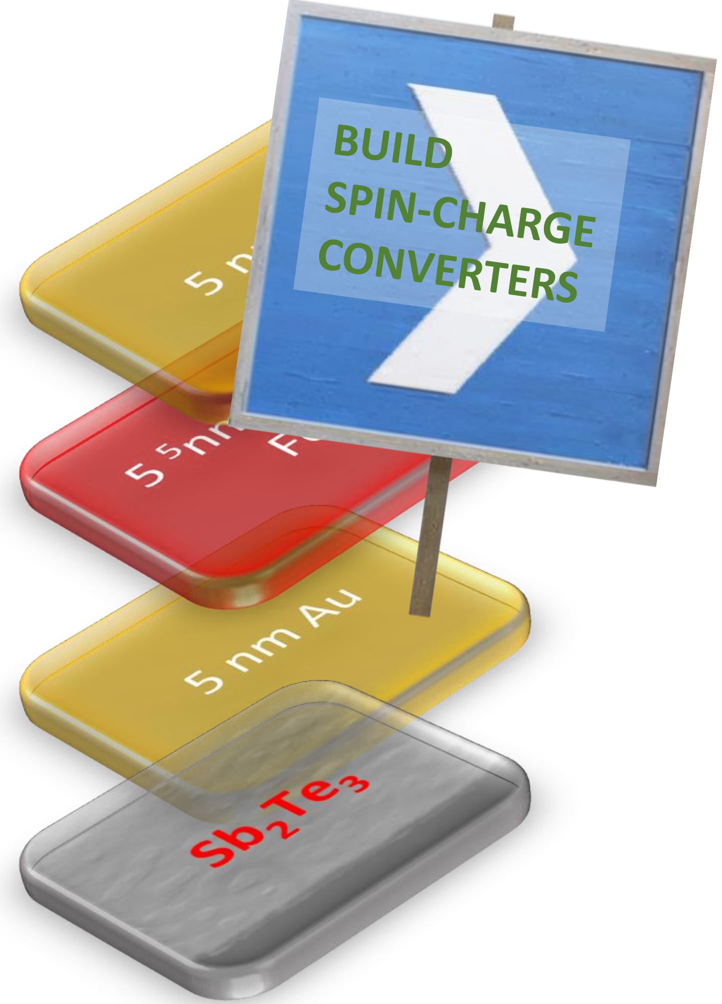

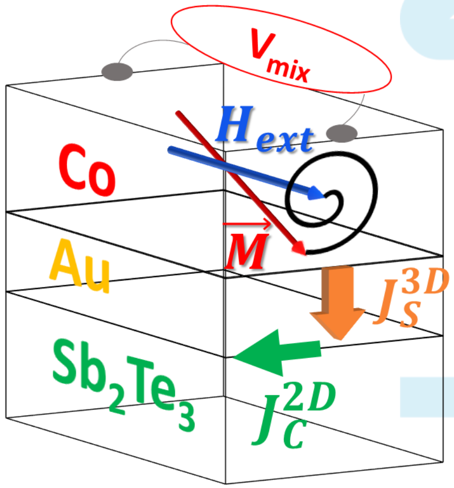

Set of samples for SP-FMR

Large Spin-to-Charge Conversion at Room Temperature in Extended Epitaxial Sb_2Te_3 Topological Insulator Chemically Grown on Silicon

Emanuele Longo, Matteo Belli, Mario Alia, Martino Rimoldi, Raimondo Cecchini, Massimo Longo, Claudia Wiemer, Lorenzo Locatelli, Polychronis Tsipas, Athanasios Dimoulas, Gianluca Gubbiotti, Marco Fanciulli, and Roberto Mantovan**

ADVANCED FUNCTIONAL MATERIALS

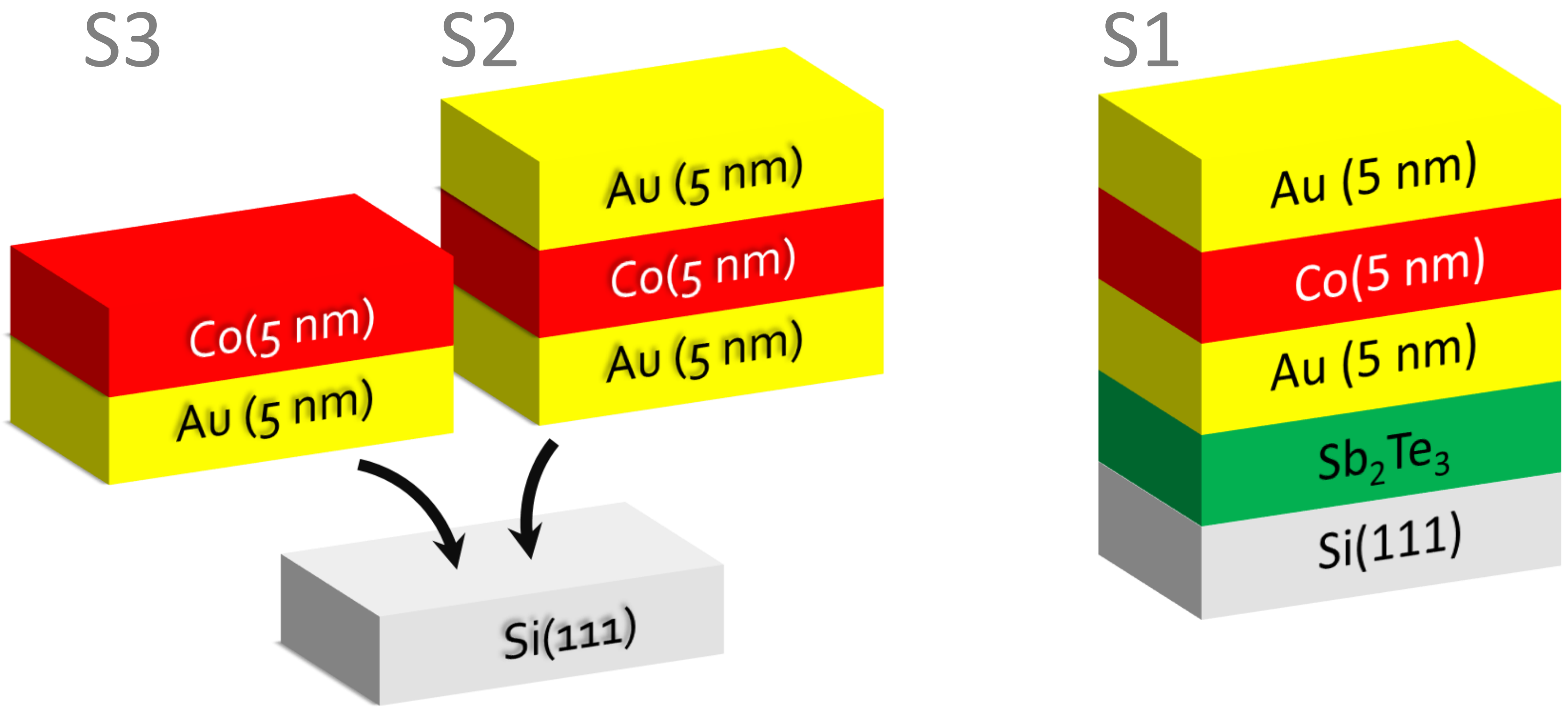

It is fundamental to grow the reference and the "functional" samples simultaneously

1) **Broadband-FMR→ Kittel (f *vs* H), damping parameter α,…**
2) **Electrically detectd SP-FMR→S2C conversion**

E. Longo et al., Adv. Funct. Mater. (2021)
E. Longo et al., Adv. Mater. Interfaces (2021)

SP-FMR in Sb_2Te_3

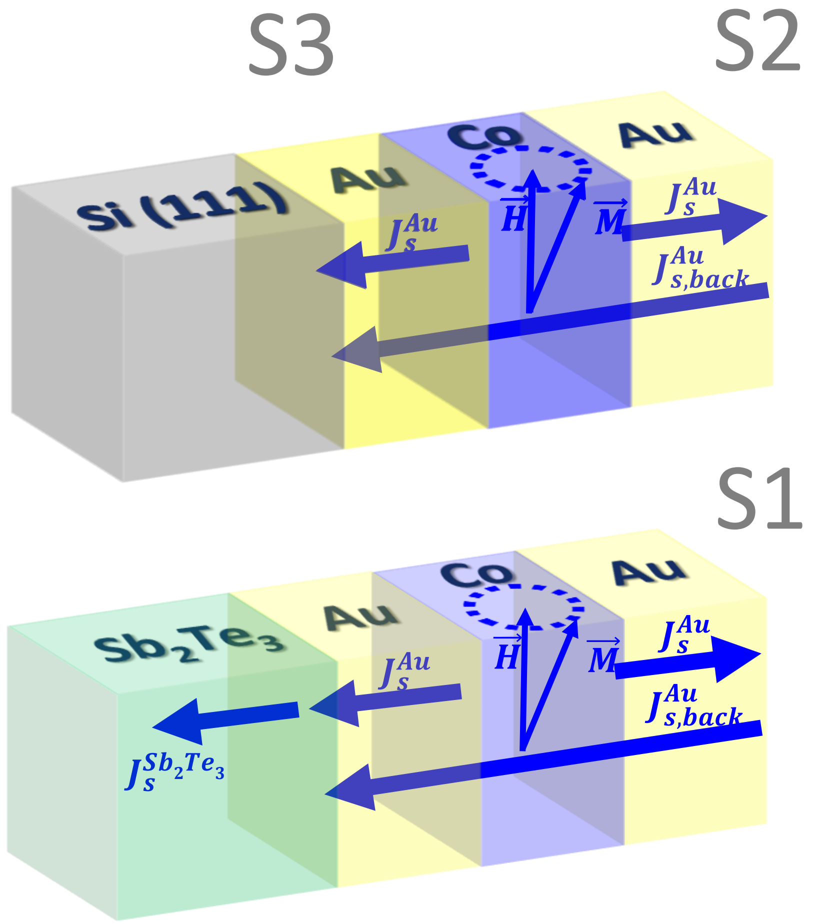

250% enhancement when compared to reference

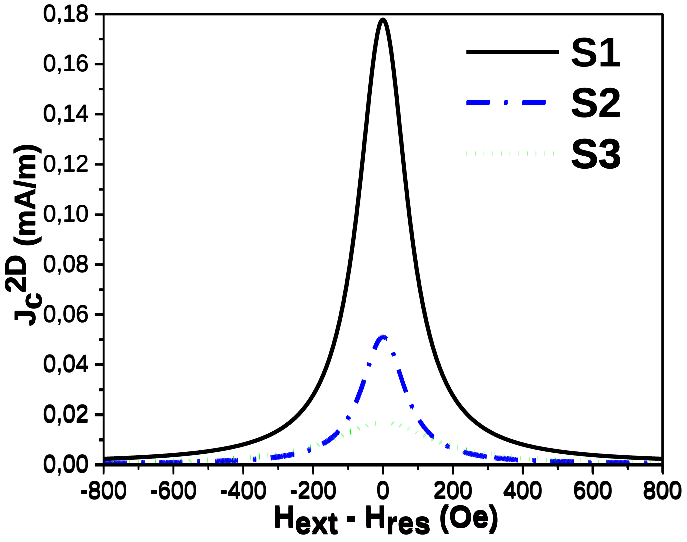

J_C^{2D}

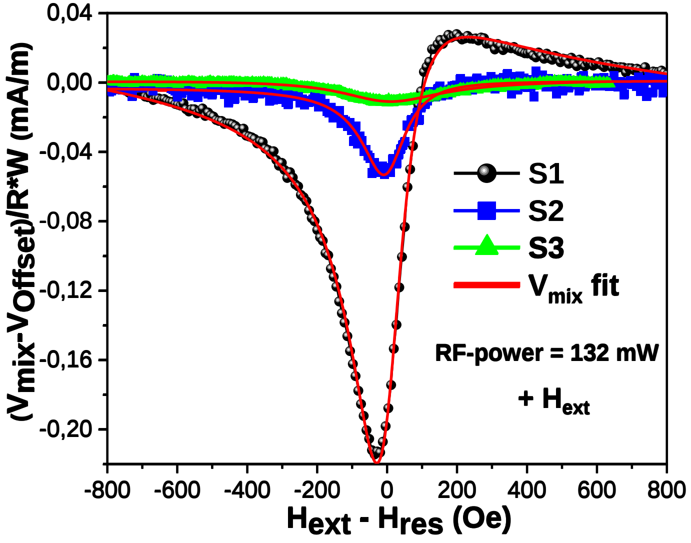

E. Longo et al., Adv. Funct. Mater. (2021)
E. Longo et al., Adv. Mater. Interfaces (2021)

2D Spin-Charge conversion at interfaces with TI

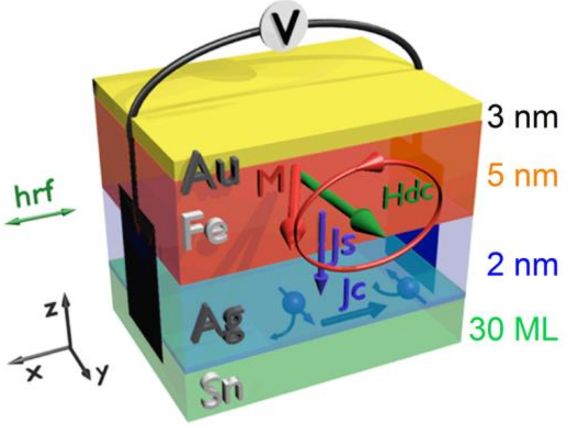

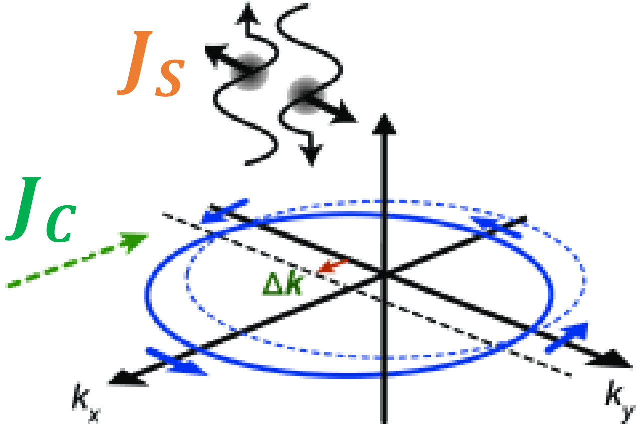

Efficiency

$$\frac{J_C}{J_S}=\lambda_{IEE}$$

Inverse Edelstein Effect (IEE)

Energy dispersion surfaces in TI

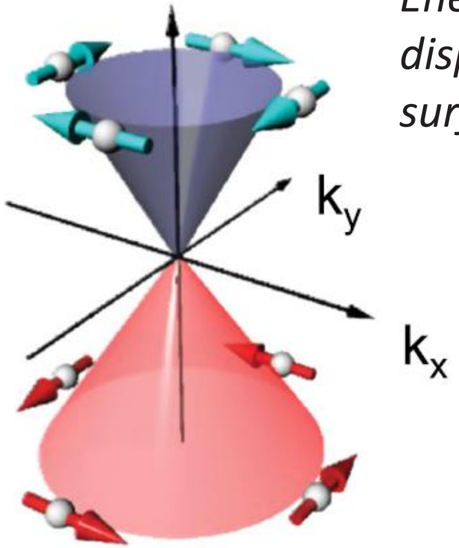

Inverse Edelstein Effect (IEE)**: Injecting a 3D-spin current density **J_S** into the surface states of a TI (along y) generates an extra population **Δk** on one side of the Fermi countours (along x) and a consequent 2D-charge current **J_C

The spin accumulation is perpendicular to current direction **(spin-momentum locking)**

Rojas-Sanchez et al, Phys. Rev. Lett. (2016); A. Soumyanarayanan et al., Nature (2016); W. Han, npj Quantum Materials (2018)

S2C Conversion efficiency

$$J_S^{3D} \begin{cases} Re(g^{\uparrow\downarrow}_{eff,Sb2Te3}) \doteq \dfrac{4\pi M_s t_{FM}}{g\mu_B}(\alpha_{S1} - \alpha_{S2}) \doteq \dfrac{2M_s t_{FM}\gamma}{g\mu_B f}(\Delta H_{S1} - \Delta H_{S2}) \\ J_S^{3D} = \dfrac{Re(g^{\uparrow\downarrow}_{eff})\gamma^2 h_{RF}^2 \hbar}{8\pi\alpha^2}\left(\dfrac{\mu_0 M_S - \sqrt{(\mu_0 M_S)^2 + 4\omega^2}}{(4\pi M_S\,\gamma)^2 + 4\omega^2}\right)\dfrac{2e}{\hbar} \end{cases}$$

@Fixed 10.5 GHz

(from Broadband-FMR)

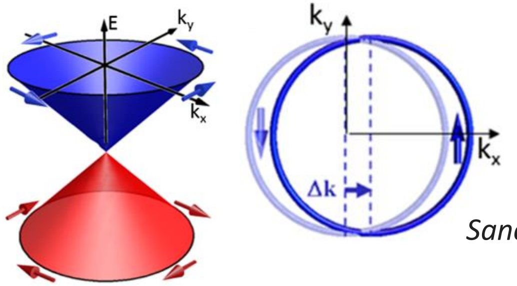

Sanchez et al, PRL (2016)

$$\lambda_{IEE} = \frac{J_C^{2D}}{J_S^{3D}} = 0.28 \text{ nm}$$

(**0.61 nm** if within single frequency approach)

Material	Growth of HM or TI	$g_{eff}^{\uparrow\downarrow}$ (m^{-2})	λ_{IEE} (nm)	Ref.
Sb_2Te_3(30nm)/Au/Co	**MOCVD**	0.834×10^{19}	**0.28**	**Our work**
Sb_2Te_3(30nm)/Au/Fe	**MOCVD**	0.53×10^{19}	**0.27**	**Our work**
α-Sn/(Ag/)/Fe	MBE	-	**2.1**	Sanchez 2016 PRL
Ag/Bi	MBE	1.29-3.21 $*10^{19}$	**0.2-0.33**	Sanchez 2016 Nat Comm
$Bi_{43}Se_{57}$(12-2nm)/CoFeB	Sputtering	~0.7 $*10^{19}$	**0.1-0.32**	Mahendra 2019 Nano Lett
Bi_2Se_3/Bi/Fe	MBE	~2.5 - 16.57 $\times 10^{20}$	**0.125-0.28**	Sun 2019 Nano Lett

Competitive to S2C in system produced by sputtering and MBE

E. Longo et al., Adv. Funct. Mater. (2021)
E. Longo et al., Adv. Mater. Interfaces (2021)

Spin-Charge converter based on Sb_2Te_3/Bi_2Te_3

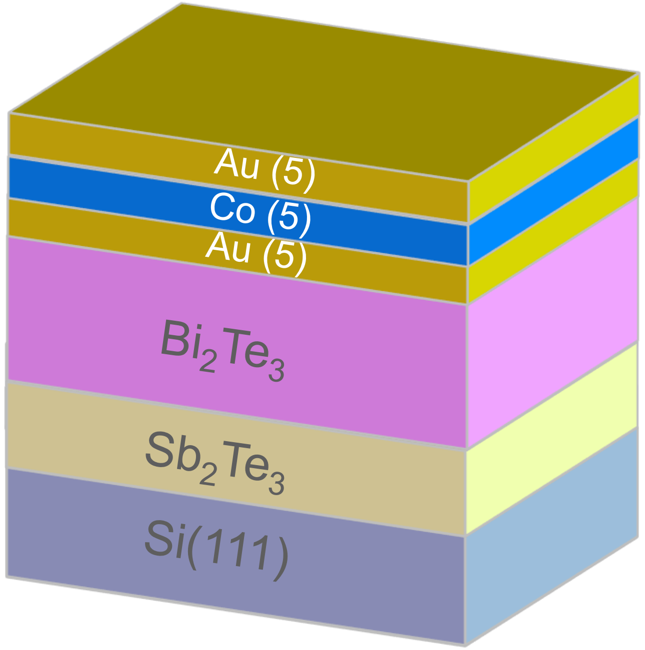

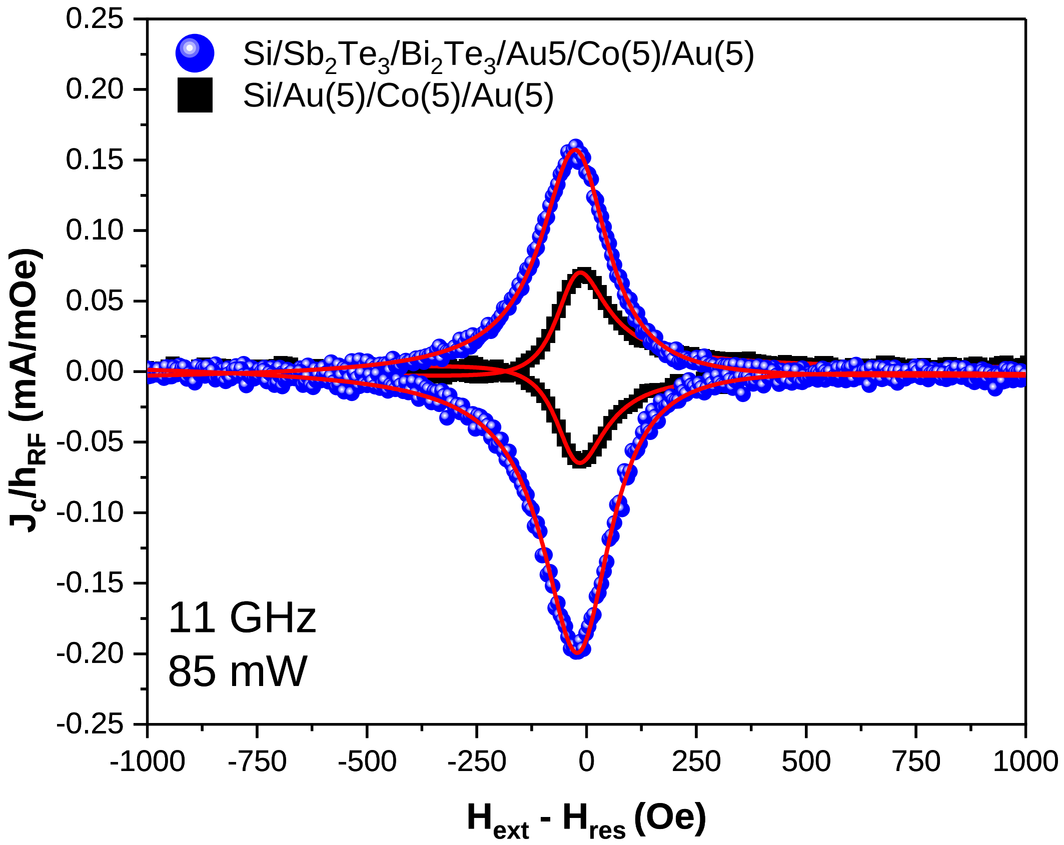

SP-FMR at room temperature

The **reference** Au/Co/Au sample is **simultaneously deposited** with the Sb_2Te_3/Bi_2Te_3 one

$$\lambda_{IEE} = \frac{J_C^{2D}}{J_S^{3D}} = 0.44 \text{ nm}$$

→ S2C conversion > the 0.28nm value in single Sb_2Te_3

→ Demonstrate the beneficial effect of moving E_F close to DP

E. Longo. L. Locatelli et al., ACS Appl. Mater. Interfaces (2023)

Summary

- **Motivation**
  - Topological insulators: intro and applications

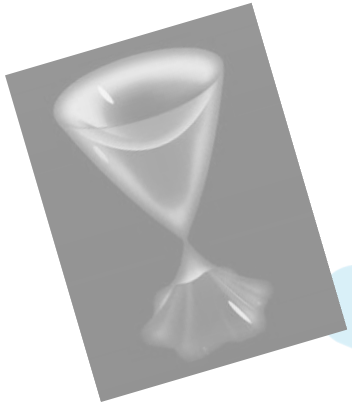

- **MOCVD of topological insulators**
  - Sb_2Te_3, Bi_2Te_3 and Sb_2Te_3/Bi_2Te_3 on large-area Si-based substrates

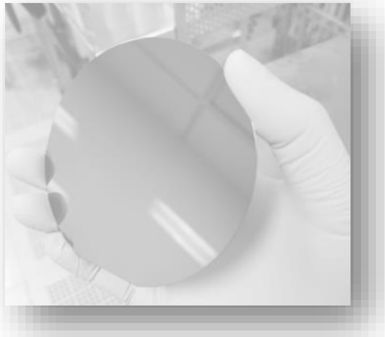

- **Spin-charge conversion in MOCVD-TIs**
  - The case of Sb_2Te_3 and Sb_2Te_3/Bi_2Te_3

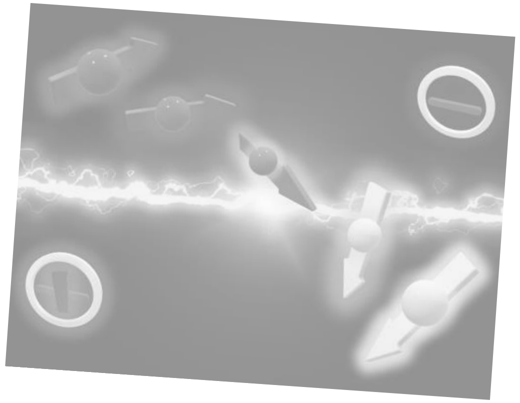

- **Conclusions & Outlook**

Conclusions

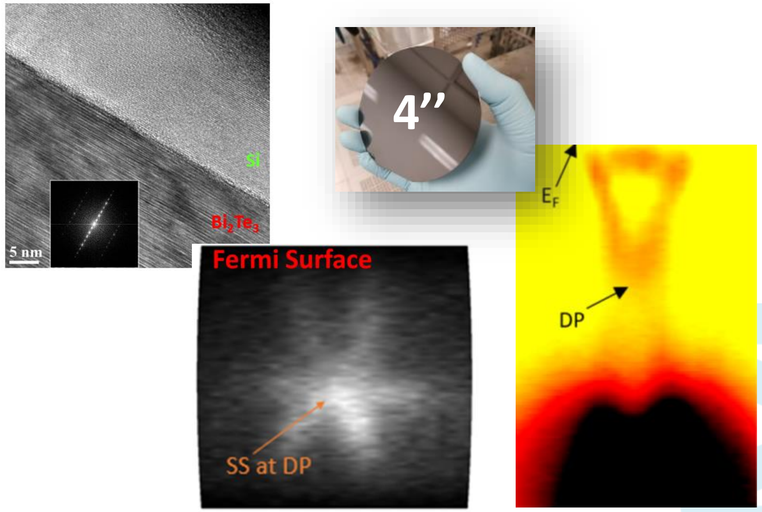

- **Large area (4'') Sb_2Te_3, Bi_2Te_3, and Sb_2Te_3/Bi_2Te_3 TIs on Si(111) by MOCVD developed**
  - Epitaxial quality
  - Topology verified (ARPES, MR)

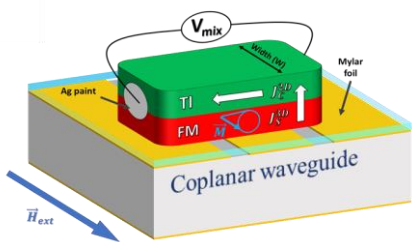

- **Very efficient spin-charge conversion observed in Sb_2Te_3 and Sb_2Te_3/Bi_2Te_3**
  - Importance of protecting the TSS with interlayers (here Au)
  - SCC efficiency comparable to state of the art methods (MBE, sputtering,…)

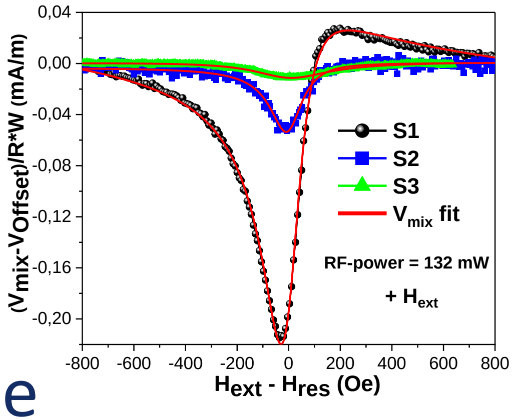

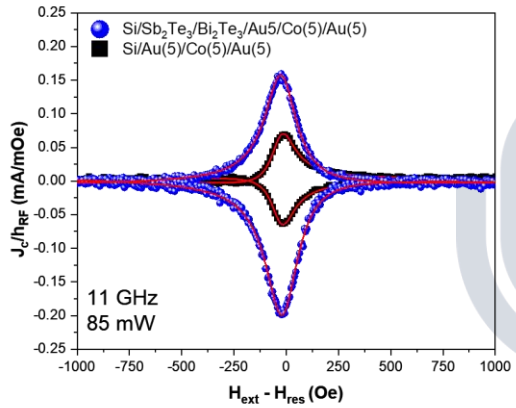

Opportunities at ISOLDE? Magnetic TIs

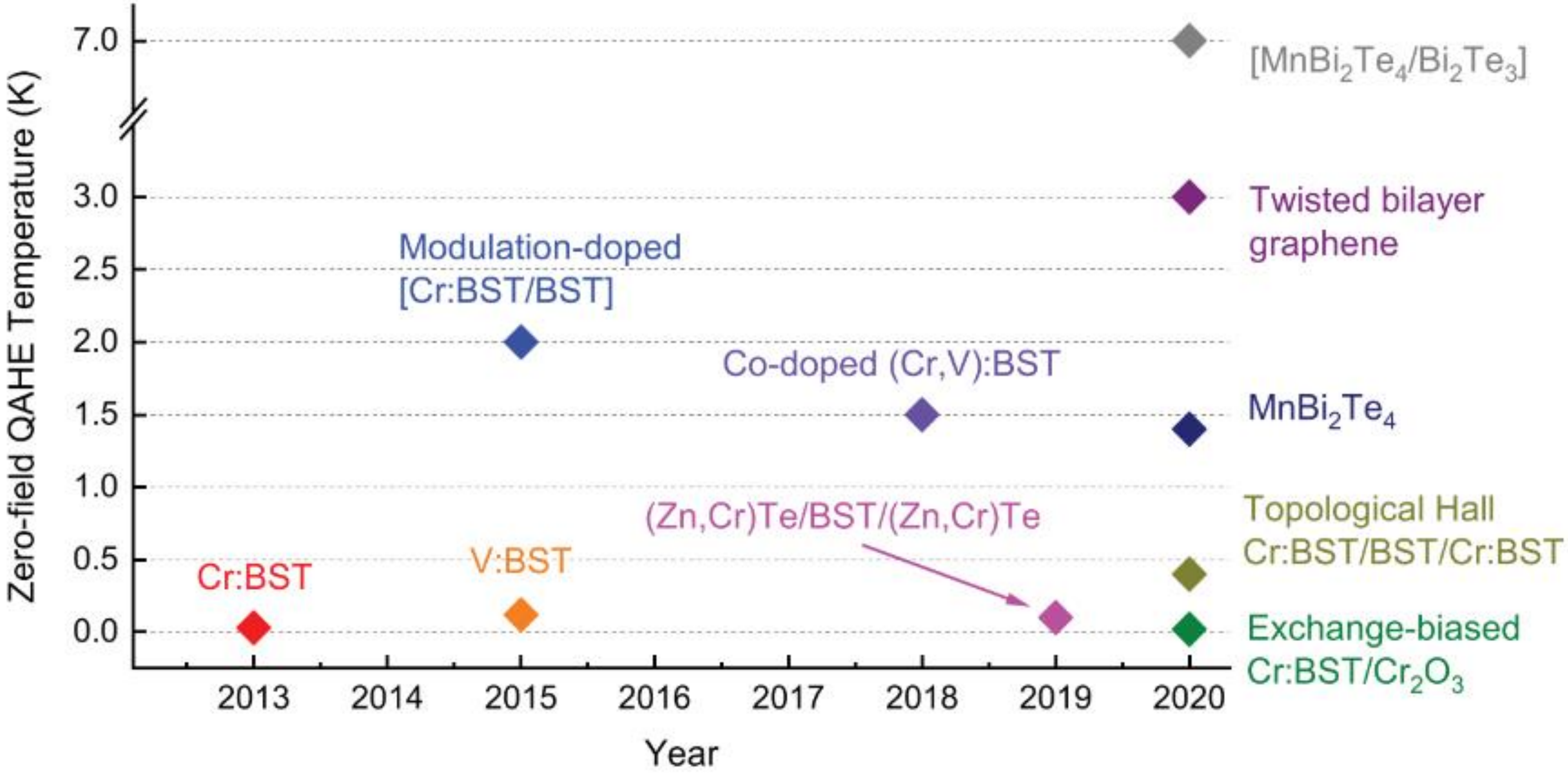

Figure 2. Timeline of the temperature performance of QAHE quantum materials (at zero external field). 2013: Cr-doped BST film at 30 mK;[22] 2015: V-doped BST film at 120 mK,[29] and modulation-doped [Cr:BST/BST] heterostructure at 2 K;[30] 2018: Co-doped (Cr,V):BST film at 1.5 K;[31] 2019: MI/TI/MI sandwich structure (Zn,Cr)Te/BST/(Zn,Cr)Te at 100 mK;[32] 2020: twisted bilayer graphene at 3 K,[34] intrinsic magnetic TI $MnBi_2Te_4$ flakes at 1.4 K,[35] [$MnBi_2Te_4/Bi_2Te_3$] superlattice at 7 K,[36] Cr:BST/BST/Cr:BST sandwich structure at 0.4 K (which also demonstrates the topological Hall effect[232]), and Cr:BST/Cr_2O_3 heterostructure at 20 mK (which also demonstrates exchange bias[33]).

Liu at al, "Magnetic Topological Insulator Heterostructures: A Review". Adv. Mat. (2023)

Opportunities at ISOLDE? Magnetic 2D materials

Chalcogenides	$Cr_2Ge_2Te_6$, $Cr_2Si_2Te_6$, Fe_3GeTe_2, VSe_2^*, $MnSe_x^*$	$Fe_2P_2S_6$, $Fe_2P_2Se_6$, $Mn_2P_2S_6$, $Mn_2P_2Se_6$, $Ni_2P_2S_6$, $Ni_2P_2Se_6$, $CuCrP_2Se_6^*$, $AgVP_2S_6$, $AgCrP_2S_6$, $CrSe_2$, $CrTe_3$, $Ni_3Cr_2P_2S_9$, $MnBi_2Te_4^*$, $MnBi_2Se_4^*$	$CuCrP_2S_6$
Halides	CrI_3^*, $CrBr_3$, GdI_2	$CrCl_3$, $FeCl_2$, $FeBr_2$, FeI_2, $MnBr_2$, $CoCl_2$, $CoBr_2$, $NiCl_2$, VCl_2, VBr_2, VI_2, $FeCl_3$, $FeBr_3$, CrOCl, CrOBr, CrSBr, $MnCl_2^*$, VCl_3^*, VBr_3^*	$CuCl_2$, $CuBr_2$, $NiBr_2$, NiI_2, CoI_2, MnI_2 α-$RuCl_3$
Others	VS_2, InP_3, GaSe, GaS	MnX_3 (X = F, Cl, Br, I), FeX_2 (X = Cl, Br, I), MnSSe, $TiCl_3$, VCl_3	SnO, GeS, GeSe, SnS, SnSe, GaTeCl, CrN, CrB_2

These inter/intra-layers coupling leads to a plethora of new magneto-optical/electrical effects

Gong et al, Science (2019) → today >1000 citations

Topological Materials Database launched

MAX PLANCK INSTITUTE
of Microstructure Physics

INSTITUTE | RESEARCH | IMPRS-STNS | CAREER | NEWS | EVENTS

FEBRUARY 26, 2019

Research

A catalogue of topological materials: insulators and semimetals characterized through topological quantum chemistry. Topological Materials Database

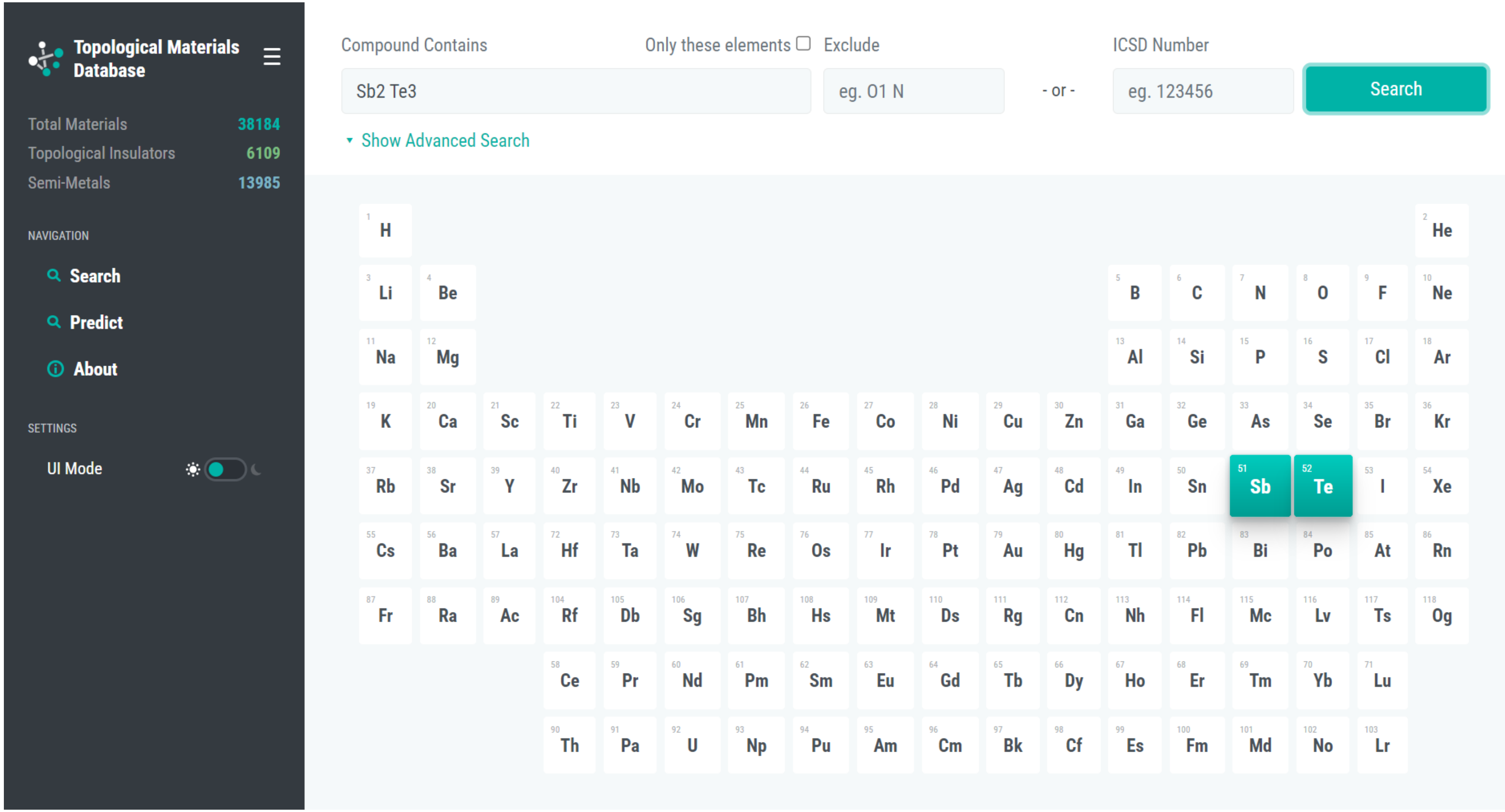

https://www.topologicalquantumchemistry.com/#/

Thank you

roberto.mantovan@cnr.it

EXTRA SLIDES

Technology Roadmap for spintronic devices

Guo et al., PROCEEDINGS OF THE IEEE 109(8), 2021

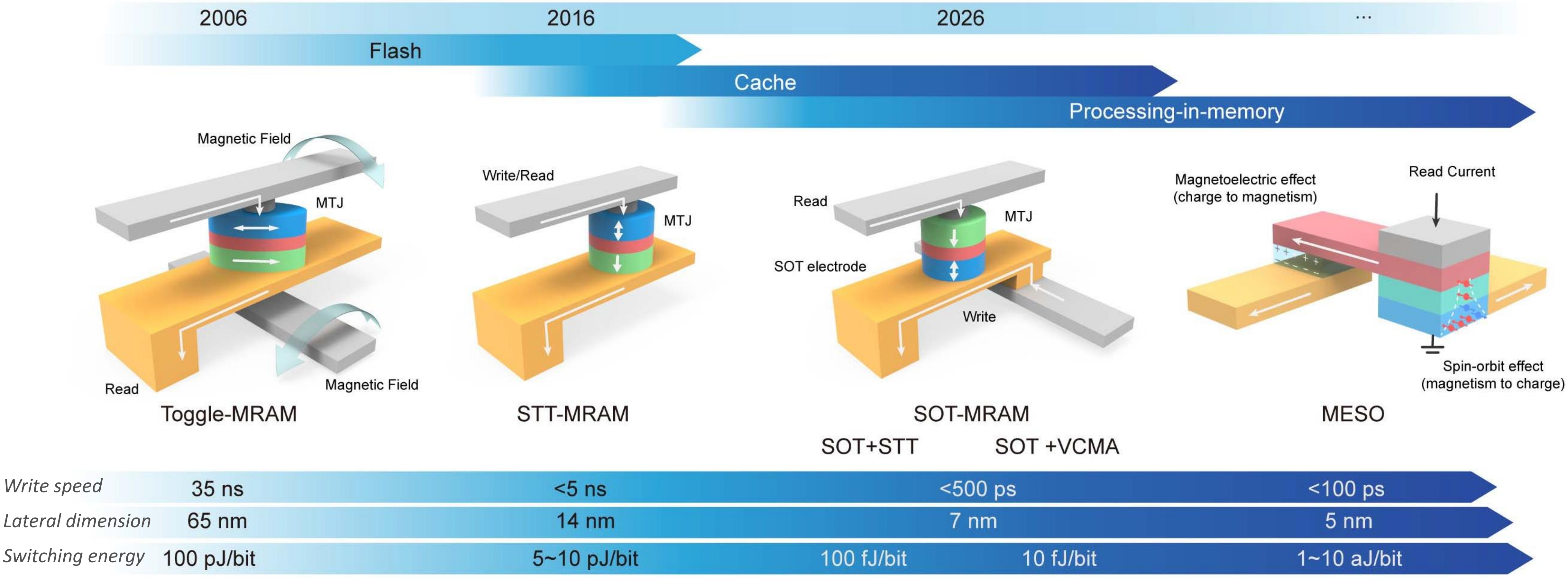

1st MRAM generation (some "niche" applications)

Everspin and Samsung: 1-Gb STT-MRAM on 28-nm CMOS (2019)
GlobalFoundries: 22-nm 40-Mb embedded STT-MRAM (2020)

IMEC: 210-ps ultrafast switching with p-MTJs in a 300-mm wafer, with high endurance (>5 × 10^{10}) and very low operation power 350 fJ/bit (2018)

3D - Topological insulators

Electrical conduction

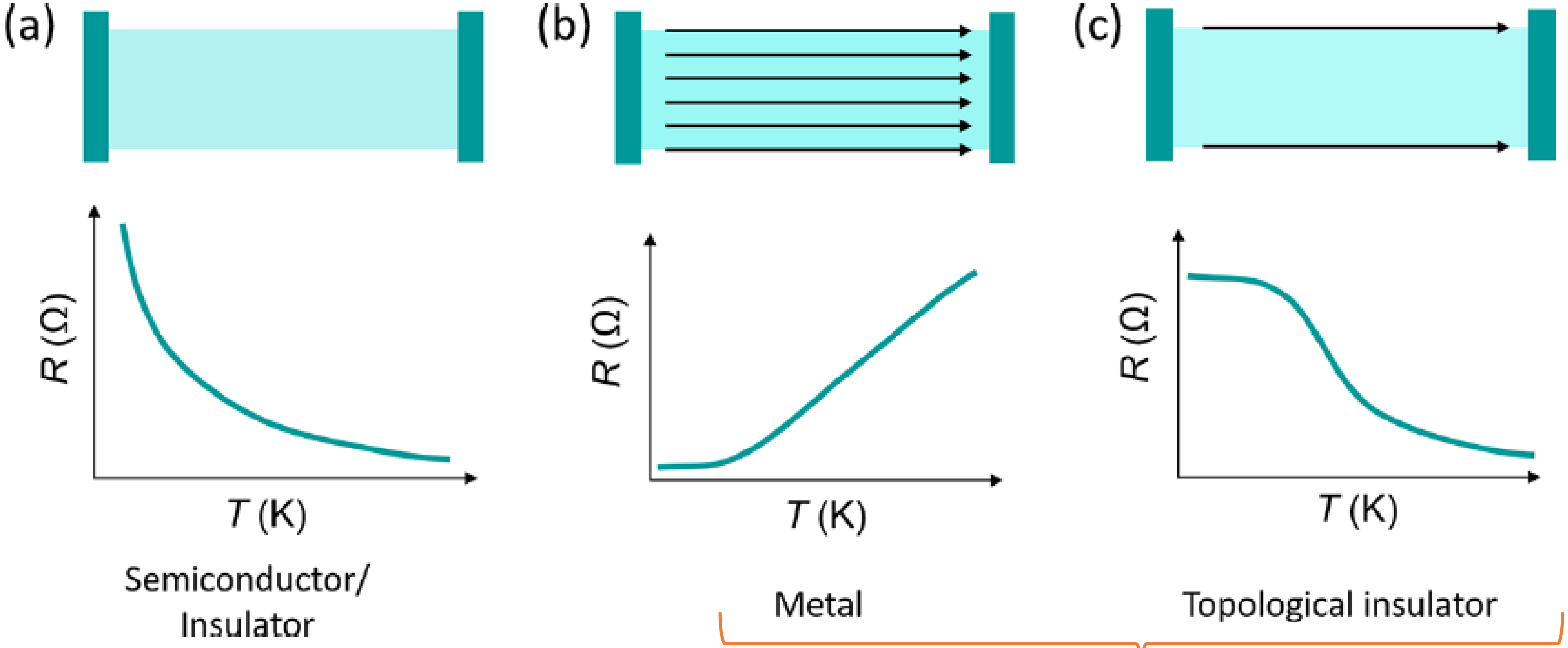

Typically coexisting….

IMM Consiglio Nazionale delle Ricerche
Institute for Microelectronics and Microsystems

Kumar et al, "Topological Quantum Materials from the Viewpoint of Chemistry" Chemical Reviews (2021)

Broadband Ferromagnetic Resonance (BFMR)

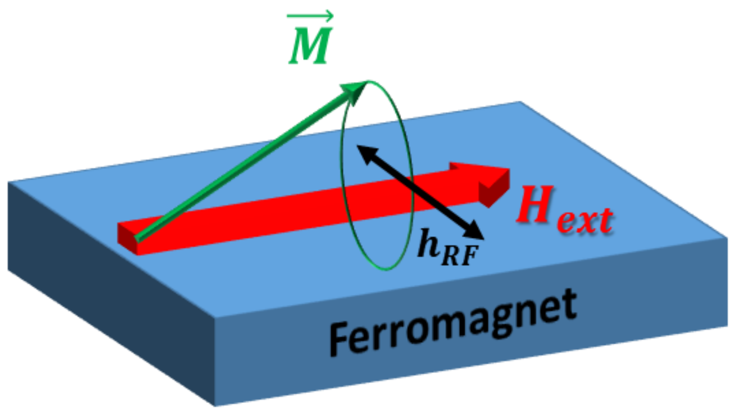

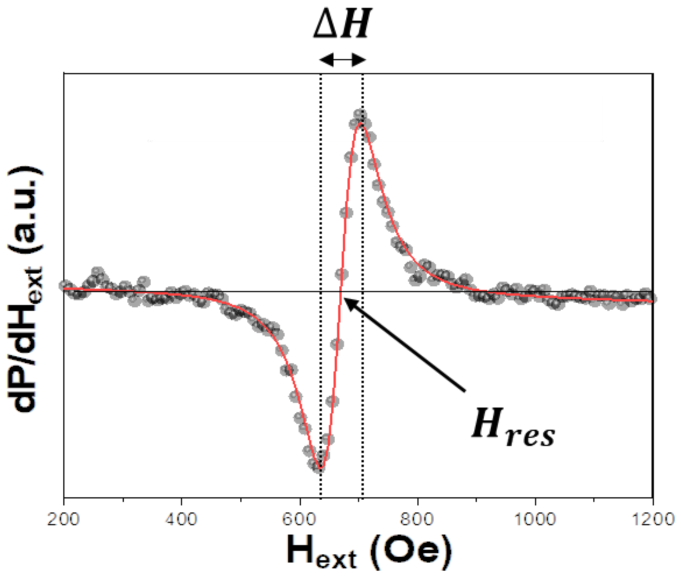

Kittel equation

$$f_{res} = \frac{\gamma}{2\pi}\sqrt{H_{res}\,(H_{res} + 4\pi M_{eff})}$$

$$4\pi M_{eff} = 4\pi M_s - H_k = 4\pi M_s - \frac{2K_s}{M_s t_{FM}}$$

Effective Magnetization

Saturation Magnetization

Anisotropy field

Ferromagnet thickness

Anisotropy constant

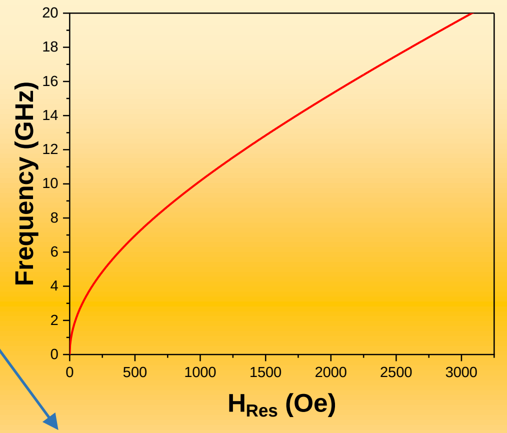

Damping constant determination (damping mechanisms of $\vec{M}$)

$$\Delta H = \Delta H_0 + \frac{4\pi}{|\gamma|}\alpha f_{res}$$

Inhomogeneous broadening (magneto-structural disorder)

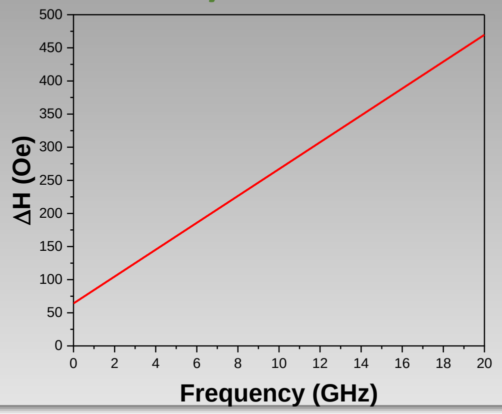

BFMR and SP-FMR set up

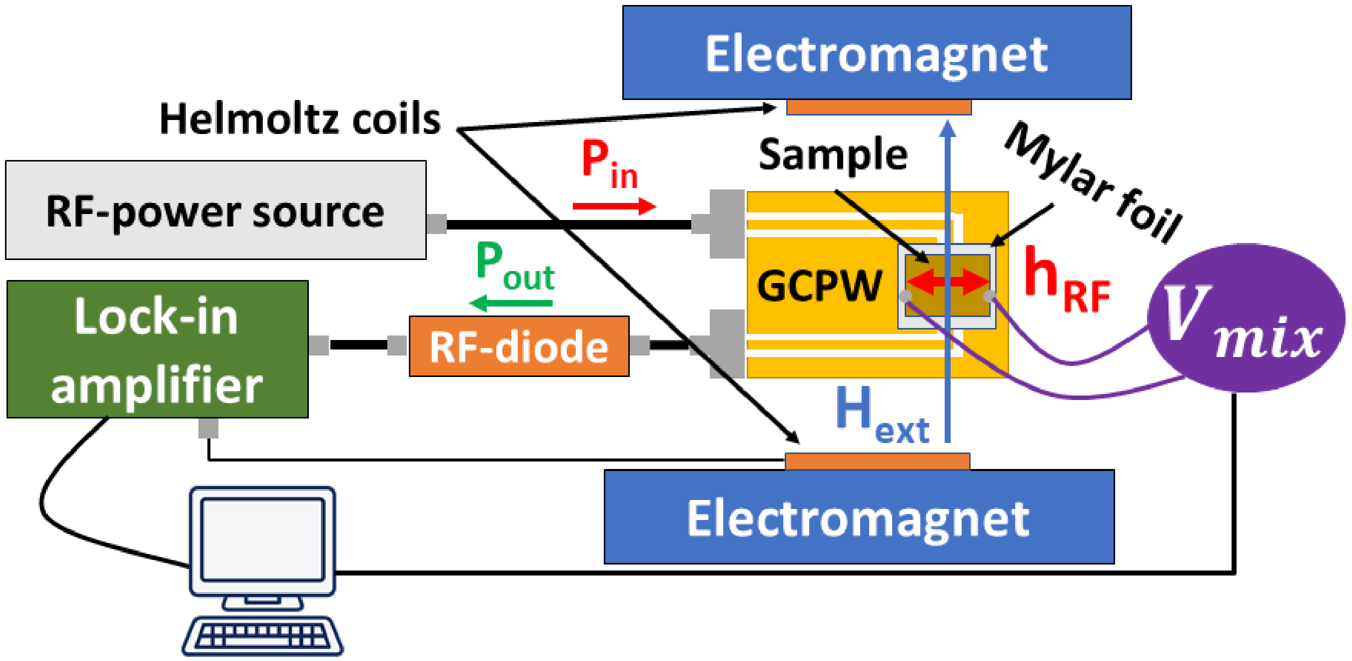

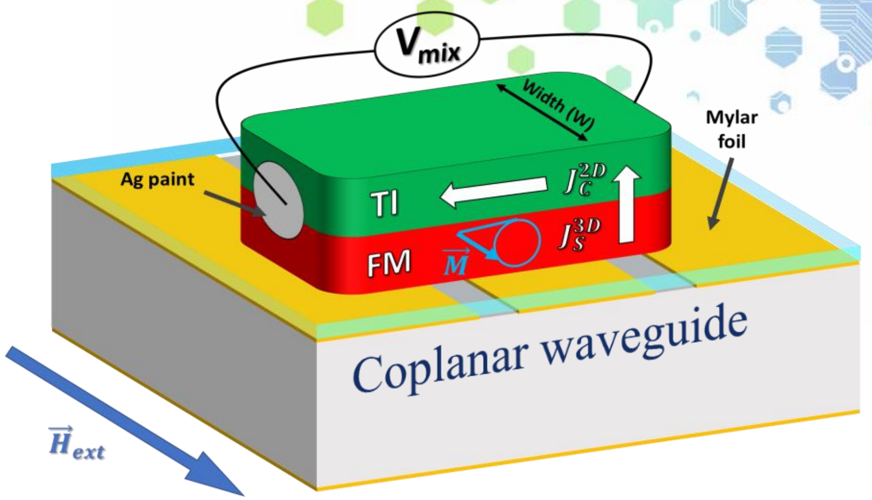

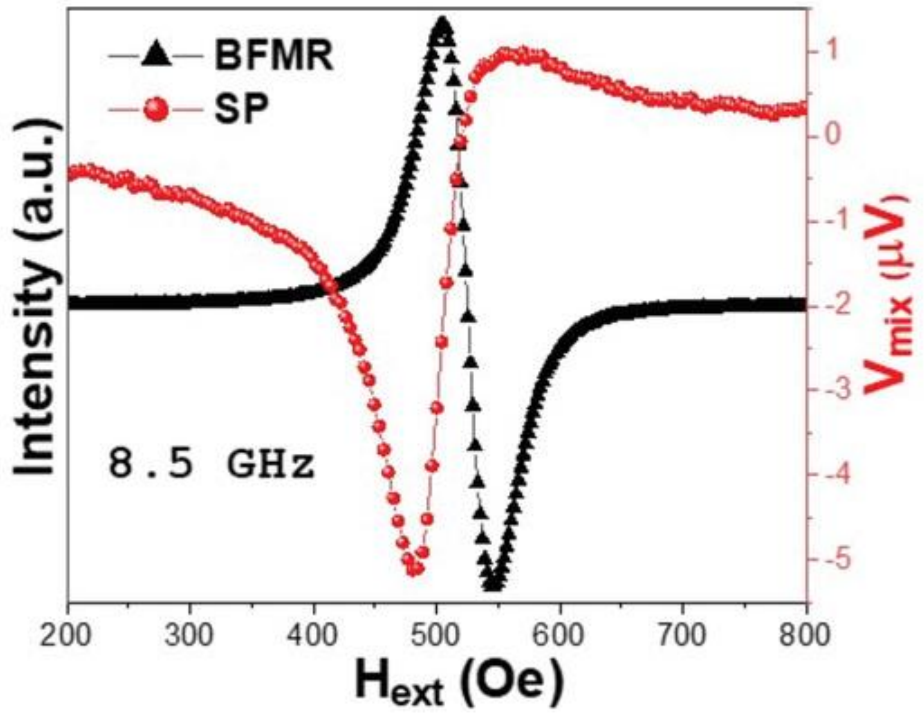

Electromagnet Poles

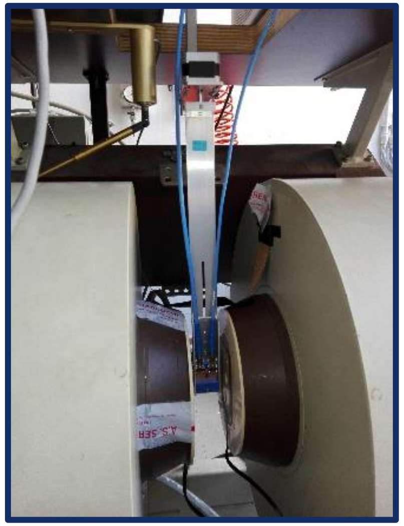

home-made CPW

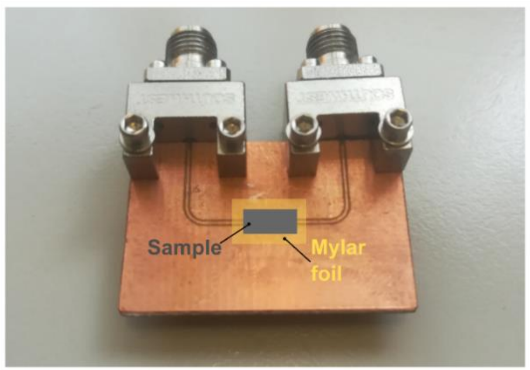

Coplanar waveguide (CPW)

BFMR first....

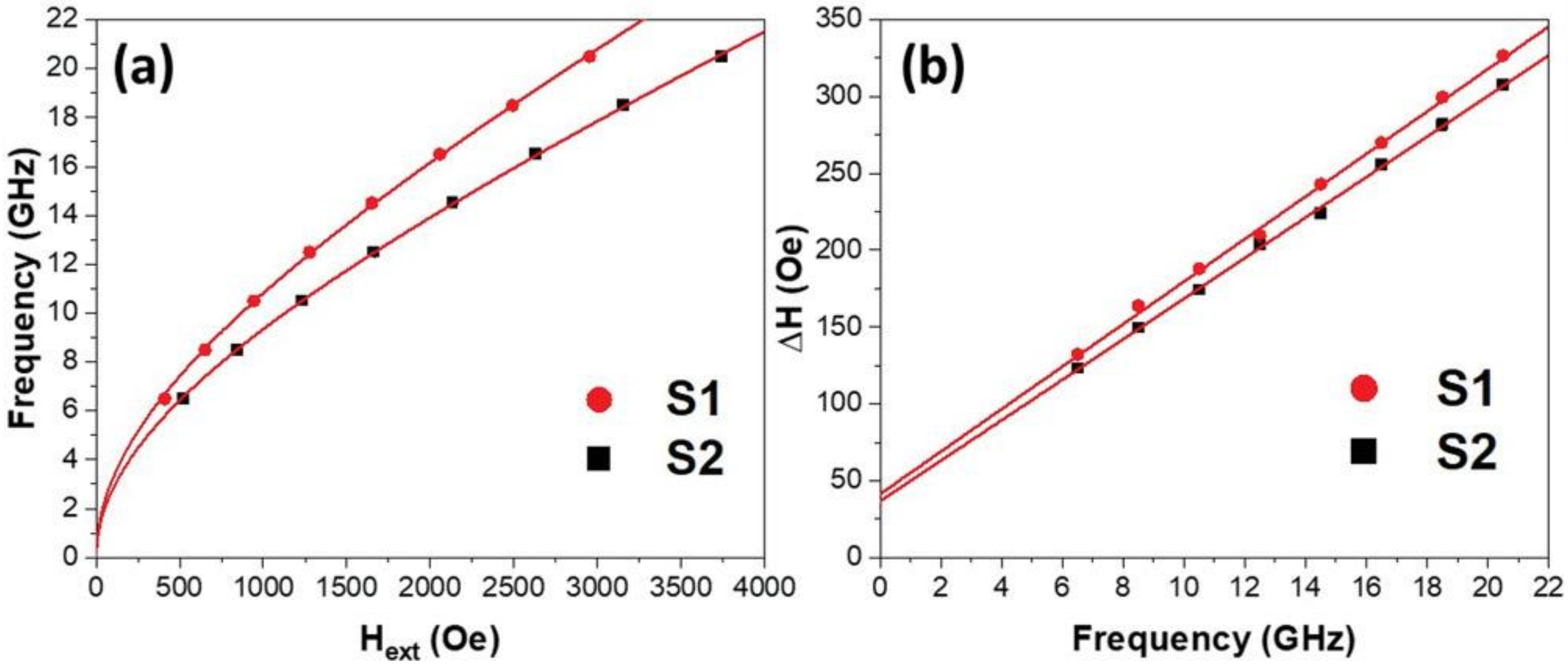

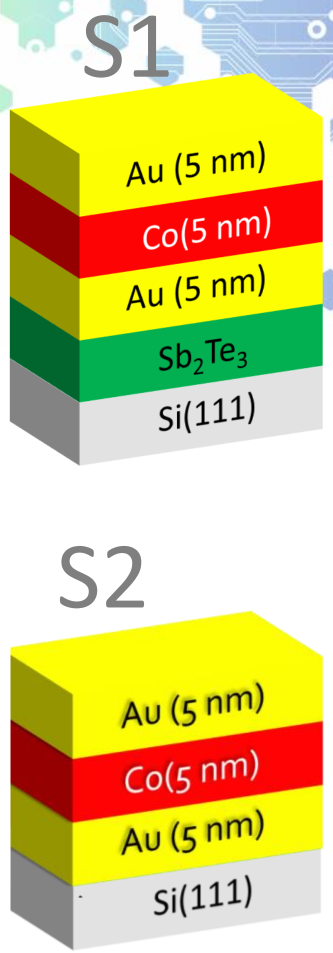

$$\Delta H = \Delta H_0 + \frac{4\pi}{|\gamma|}\alpha f_{res}$$

Broadening of the damping may suggest spin pumping in Sb_3Te_3……

Consiglio Nazionale delle Ricerche
Institute for Microelectronics and Microsystems

E. Longo et al., Adv. Funct. Mater. (2021)
E. Longo et al., Adv. Mater. Interfaces (2021)

Spin-Charge interconversion at the core of devices…

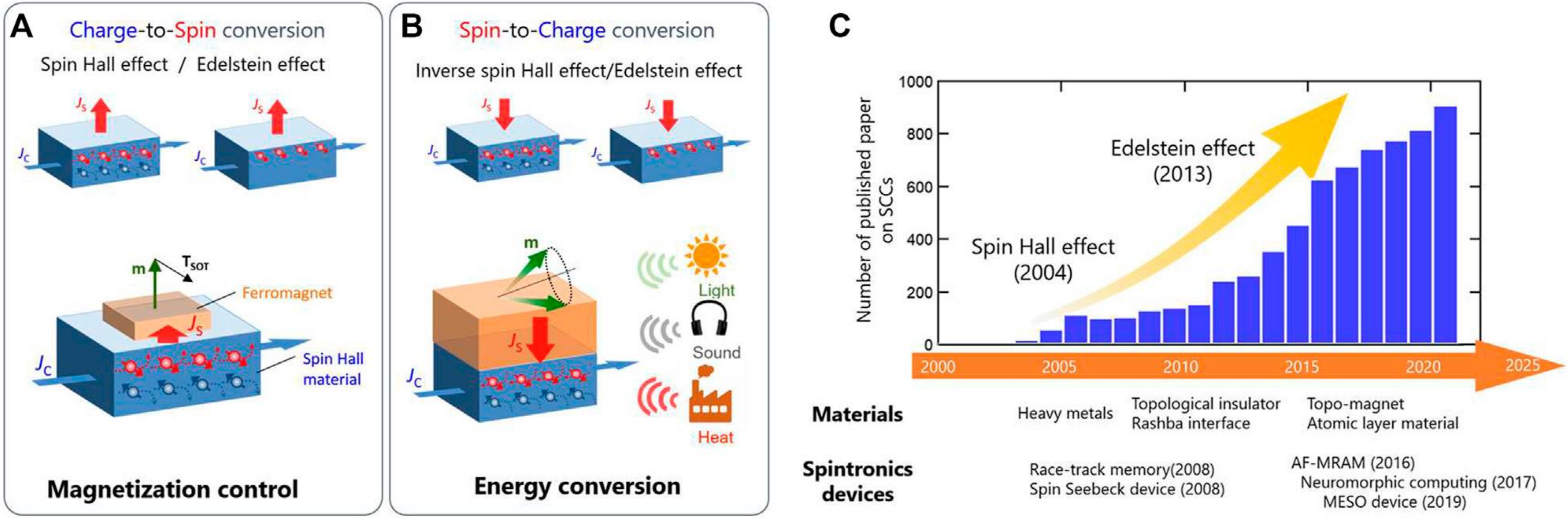

Kondou K and Otani Y, Front. Phys. 11:1140286 (2023)

3D Spin-Charge conversion

3D

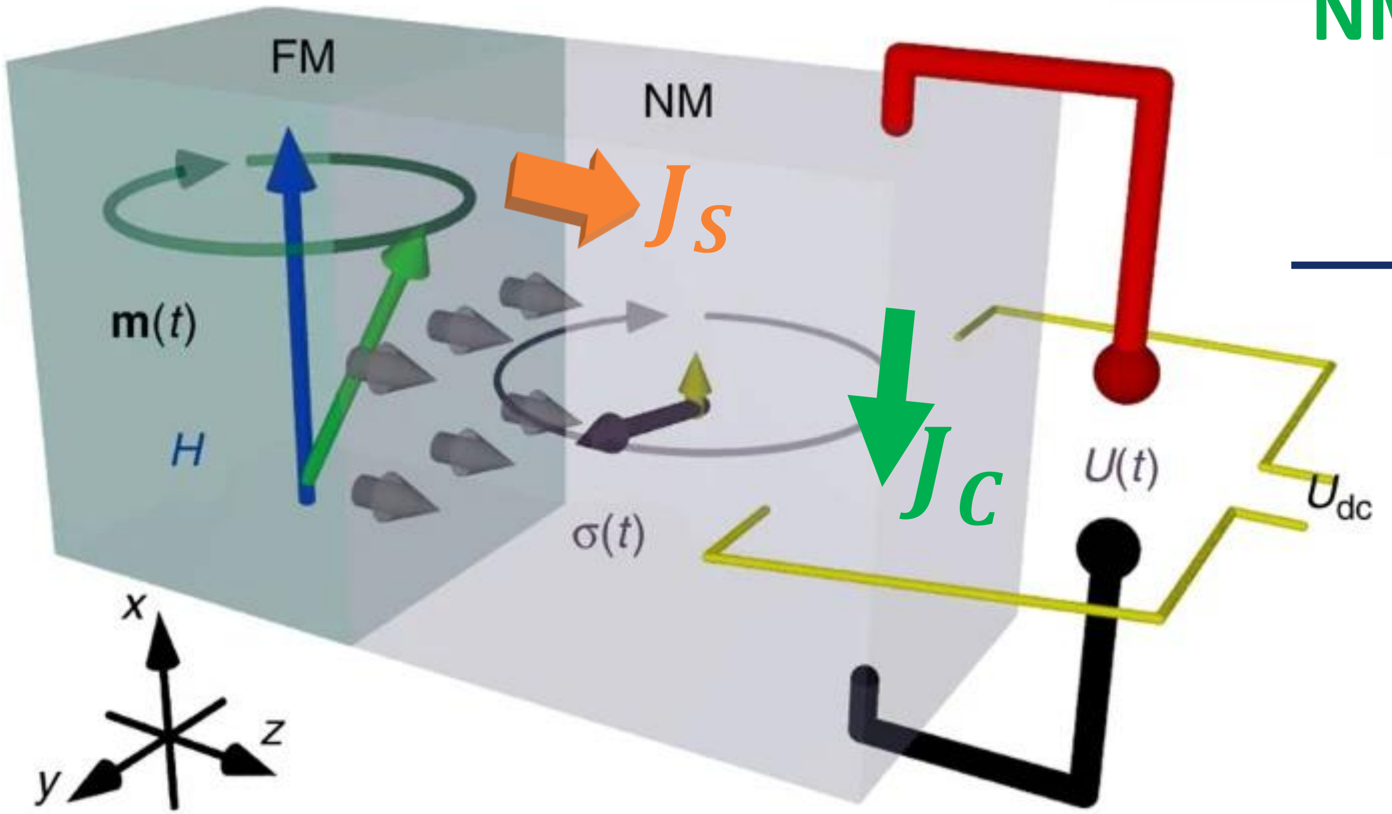

NM= Ta,Pt, …

Efficiency

$$\frac{J_C}{J_S} = \Theta_{ISHE}$$

(inverse spin Hall angle)

Conversion occurs in the bulk of the material with high SOC

Wej et al, "Spin Hall voltages from a.c. and d.c. spin currents" Nat. Comm. (2014)

2D Spin-Charge conversion

Energy dispersion surfaces

Fermi contours

*IEE: Injection of a spin current density J_S along y generates an extra population Δ**k** along x and a consequent charge current J_C*

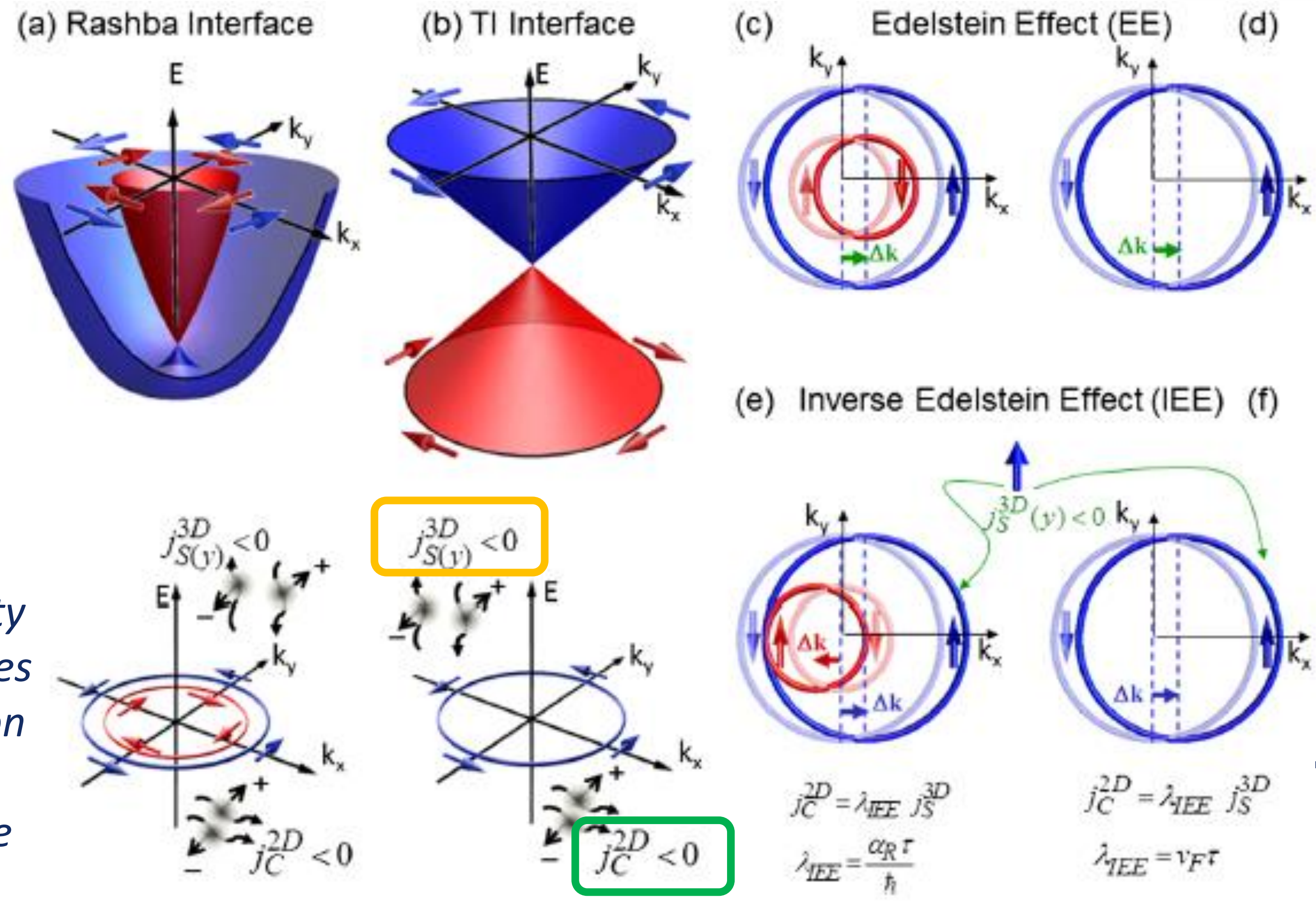

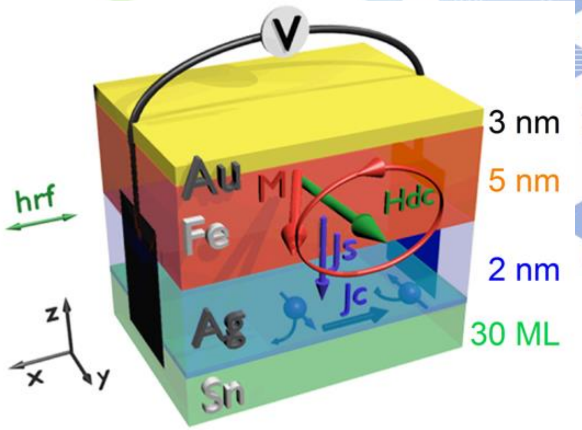

Efficiency

$$\frac{J_C}{J_S} = \lambda_{IEE}$$

Conversion occurs at the interface with TI or Rashba systems

Rojas-Sanchez et al, "Spin to Charge Conversion at Room Temperature by Spin Pumping into a New Type of Topological Insulator: α-Sn Films" Phys. Rev. Lett. (2016)

MESO device

proposed by intel

Scalable energy-efficient magnetoelectric spin-orbit logic

2019

Sasikanth Manipatruni[1]*, Dmitri E. Nikonov[1], Chia-Ching Lin[1], Tanay A. Gosavi[1], Huichu Liu[2], Bhagwati Prasad[3], Yen-Lin Huang[3,4], Everton Bonturim[3], Ramamoorthy Ramesh[3,4,5] & Ian A. Young[1]

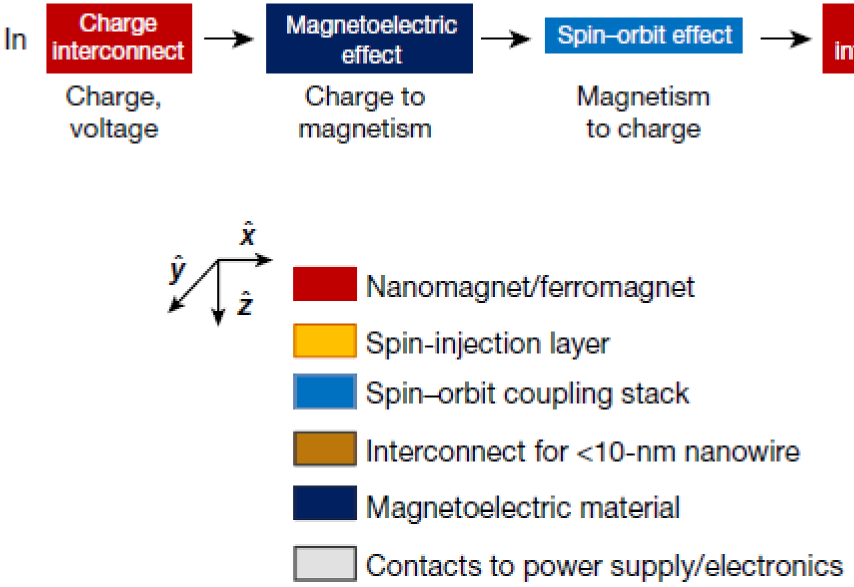

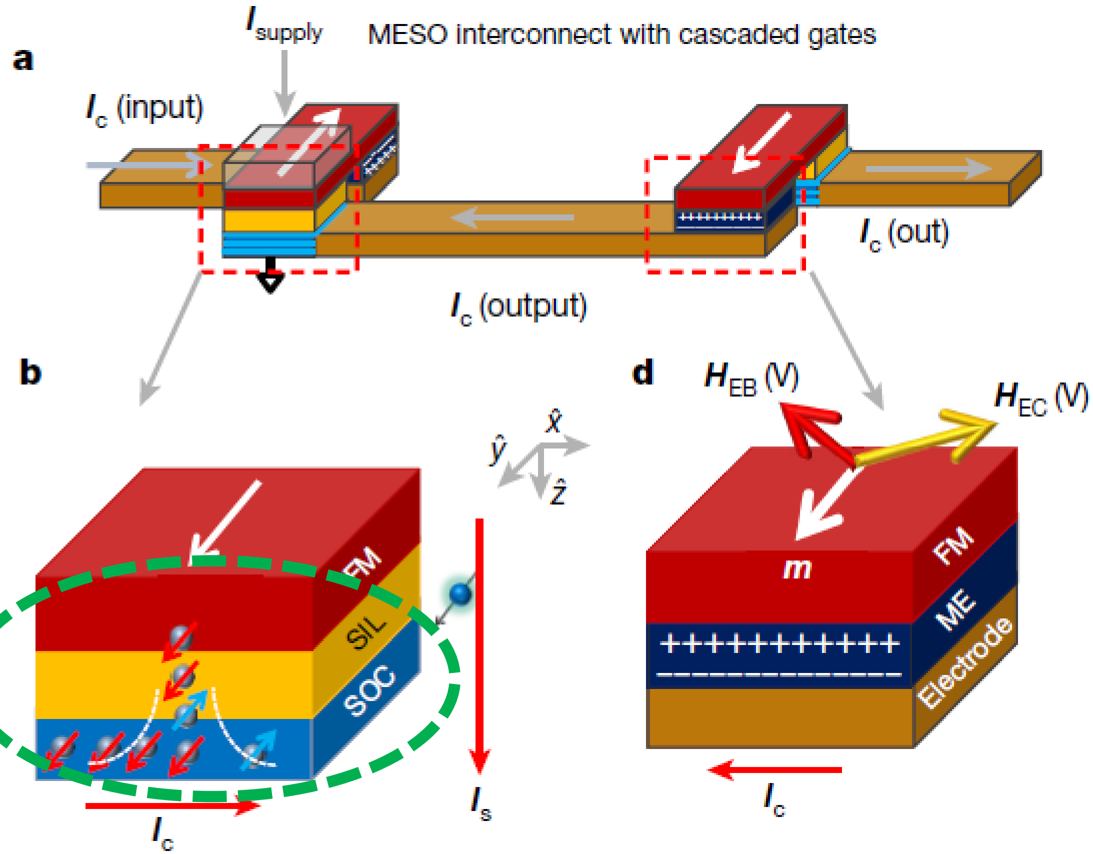

fundamental building-block

$(required\ \frac{J_C}{J_S} > 50\%)$

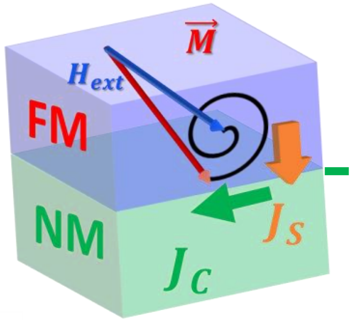

Manipatruni et al., Nature (2019)

Sb_2Te_3 by MOCVD on different substrates

The aim is to control homogenous layers with the lowest surface roughness as possible!

CRYSTAL GROWTH & DESIGN
pubs.acs.org/crystal
Article

Effect of Substrates and Thermal Treatments on Metalorganic Chemical Vapor Deposition-Grown Sb_2Te_3 Thin Films

Martino Rimoldi, Raimondo Cecchini, Claudia Wiemer, Emanuele Longo, Stefano Cecchi, Roberto Mantovan,* and Massimo Longo*

Table 1. Sb_2Te_3 Root Mean Square Roughness (R_q, nm), Measured by AFM and XRR, and Thickness (nm), Determined by XRR

	Sb_2Te_3 - as-deposited			Sb_2Te_3 - substrate annealing (*prior to growth*)			Sb_2Te_3 - post-growth annealing		
	R_q (AFM)	R_q (XRR)	thickness (XRR)	R_q (AFM)	R_q (XRR)	thickness (XRR)	R_q (AFM)	R_q (XRR)	thickness (XRR)
Si(111)[a]	3.88	3.1	33.7	1.81	2.0	32.5	1.32	1.5	32.0
Si(100)	4.80	4.6	33.7	2.78	3.4	31.0	2.26	2.6	31.7
SiO_2	2.41	3.1[b]	35.0[c]	4.90	6.6	30.9	5.51	4.5	32.4
a-Al_2O_3	3.40	3.3[d]	32.2	3.61	4.1[e]	29.0	3.07	3.4[f]	27.5
Al_2O_3(0001)	1.94	2.6	28.8	3.25	3.9[g]	28.2[h]	2.18	3.3[i]	25.2[j]

[a] Si(111) is reported for comparison purpose.[38] [b] Sb_2O_3 interlayer roughness: 0.4 nm. [c] Sb_2O_3 interlayer thickness: 2.0 nm. [d] a-Al_2O_3 roughness: 0.5 nm. [e] a-Al_2O_3 roughness: 0.4 nm. [f] a-Al_2O_3 roughness: 0.5 nm. [g] Sb_2O_3 interlayer roughness: 0.1 nm. [h] Sb_2O_3 interlayer thickness: 0.5 nm. [i] Sb_2O_3 interlayer roughness: 0.1 nm. [j] Sb_2O_3 interlayer thickness: 0.3 nm.

M. Rimoldi et al., Cryst. Growth & Design (2021)

Sb_2Te_3 by MOCVD on different substrates

Remarkable role played by pre-deposition substrate annealing and post annealing

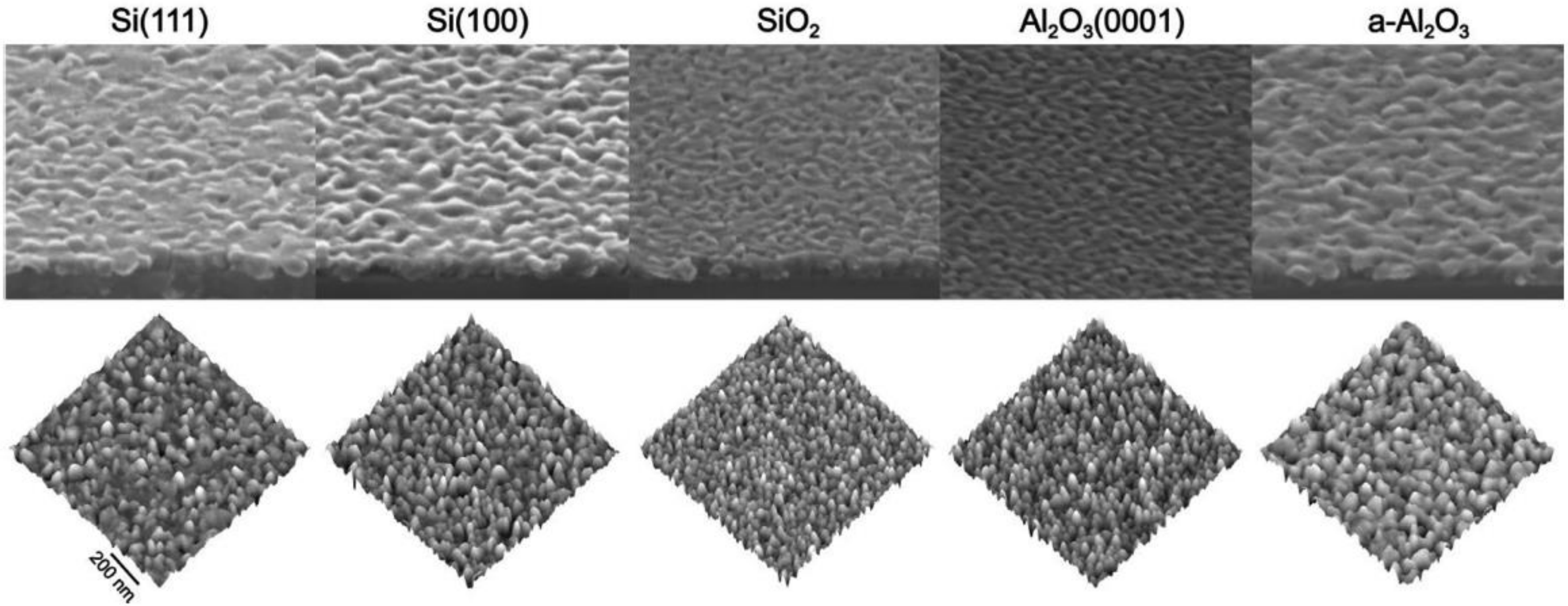

Figure 1. (top) Tilted cross-section SEM images and (bottom) AFM views of Sb_2Te_3 - *as-deposited* on (from left to right) Si(111), Si(100), SiO_2, Al_2O_3(0001), and a-Al_2O_3. Si(111) is reported for comparison purpose.[38] As-deposited films appeared to have a pronounced granularity. However, those grown on SiO_2 and Al_2O_3(0001) were significantly smoother and gave AFM R_q values of 2.41 and 1.94 nm, respectively.

AS DEPOSITED

M. Rimoldi et al., Cryst. Growth & Design (2021)

Sb_2Te_3 by MOCVD on different substrates

Remarkable role played by pre-deposition substrate annealing and post annealing

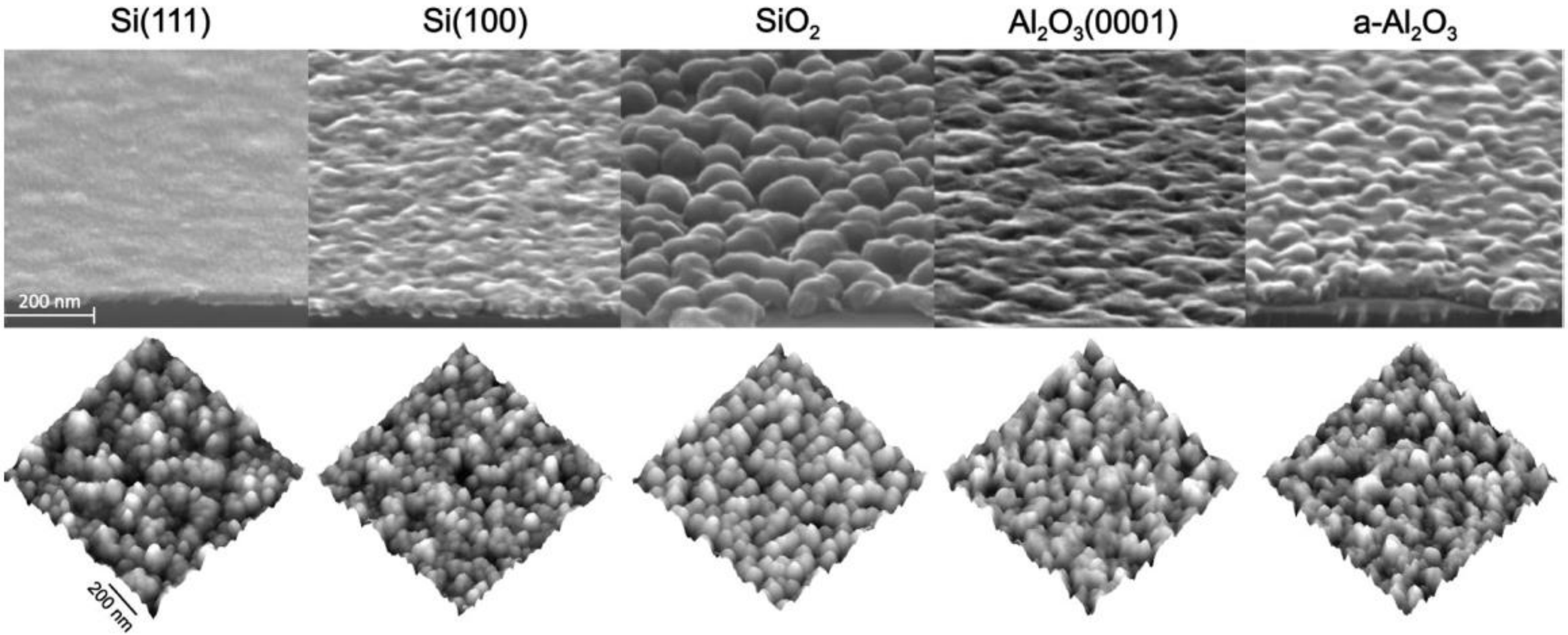

Figure 3. (top) Tilted cross-section SEM images and (bottom) AFM views of Sb_2Te_3 - *substrate annealing* on (from left to right) Si(111), Si(100), SiO_2, Al_2O_3(0001), and a-Al_2O_3. Si(111) is reported for comparison purpose.[38] The SEM images revealed the effect of substrate annealing on the morphology of the Sb_2Te_3 thin films. The granularity, and consequently the roughness, significantly improved on Si(100) and Si(111), whereas it worsened on SiO_2.

PRE-ANNEALING

M. Rimoldi et al., *Cryst. Growth & Design (2021)*

Sb_2Te_3 by MOCVD on different substrates

Remarkable role played by pre-deposition substrate annealing and post annealing

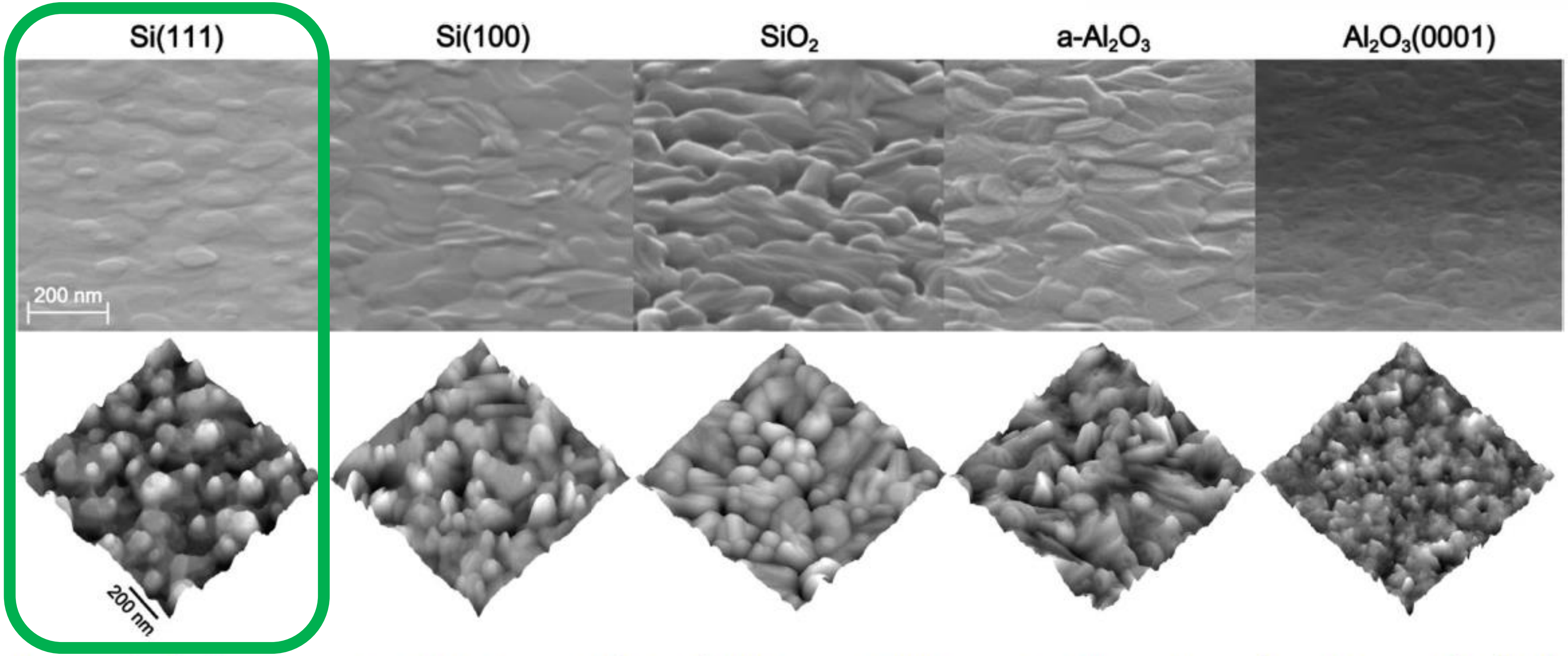

Figure 6. (top) Tilted cross-section SEM images and (bottom) AFM views of Sb_2Te_3 - *post-growth annealing* on (from left to right) Si(111), Si(100), SiO_2, a-Al_2O_3, and Al_2O_3(0001). Si(111) is shown for comparison purpose.[38] Thermal processing (post-growth annealing) induced the crystallization of the Sb_2Te_3 thin films. SEM and AFM images show the highly crystalline nature and the orientation of the films.

POST-ANNEALING

IMM Consiglio Nazionale delle Ricerche
Institute for Microelectronics and Microsystems

M. Rimoldi et al., Cryst. Growth & Design (2021)

Large-area epitaxial TIs on Si(111) are demonstrated

- TEM cross sectional view shows highly ordered crystallographic planes
- Fast Fourier Transform (FFT): identification of crystalline structure

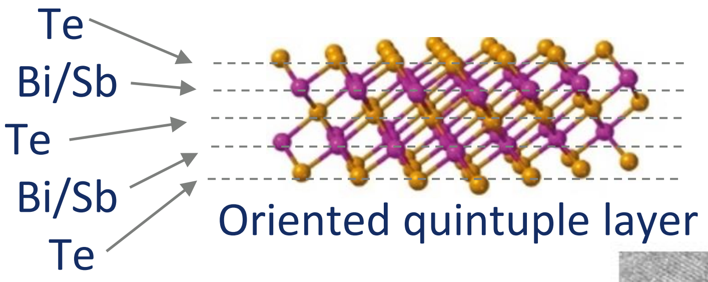

Sb_2Te_3

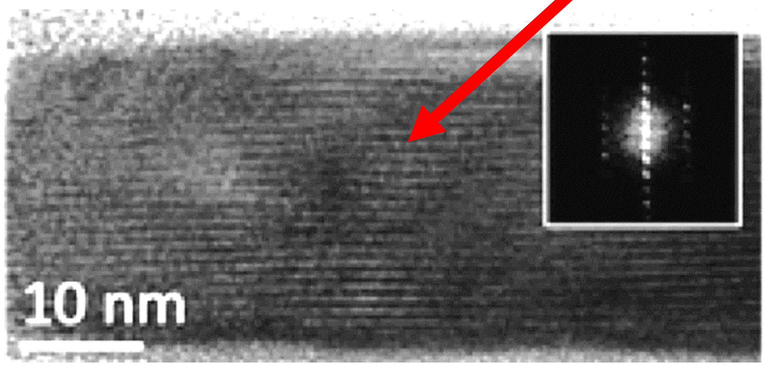

Bi_2Te_3

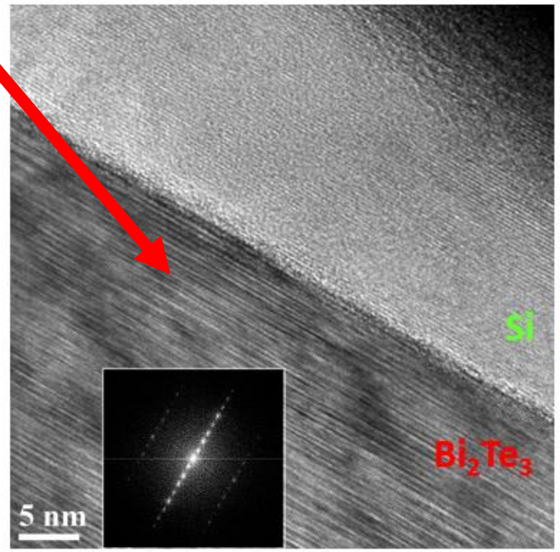

❖ FFT confirms hexagonal structure
❖ High ordered quintuple layer structure

Transport

scientific reports

OPEN

Magnetotransport and ARPES studies of the topological insulators Sb_2Te_3 and Bi_2Te_3 grown by MOCVD on large-area Si substrates

L. Locatelli[1,2✉], A. Kumar[1], P. Tsipas[3], A. Dimoulas[3], E. Longo[1] & R. Mantovan[1✉]

Sb_2Te_3: p-type conduction

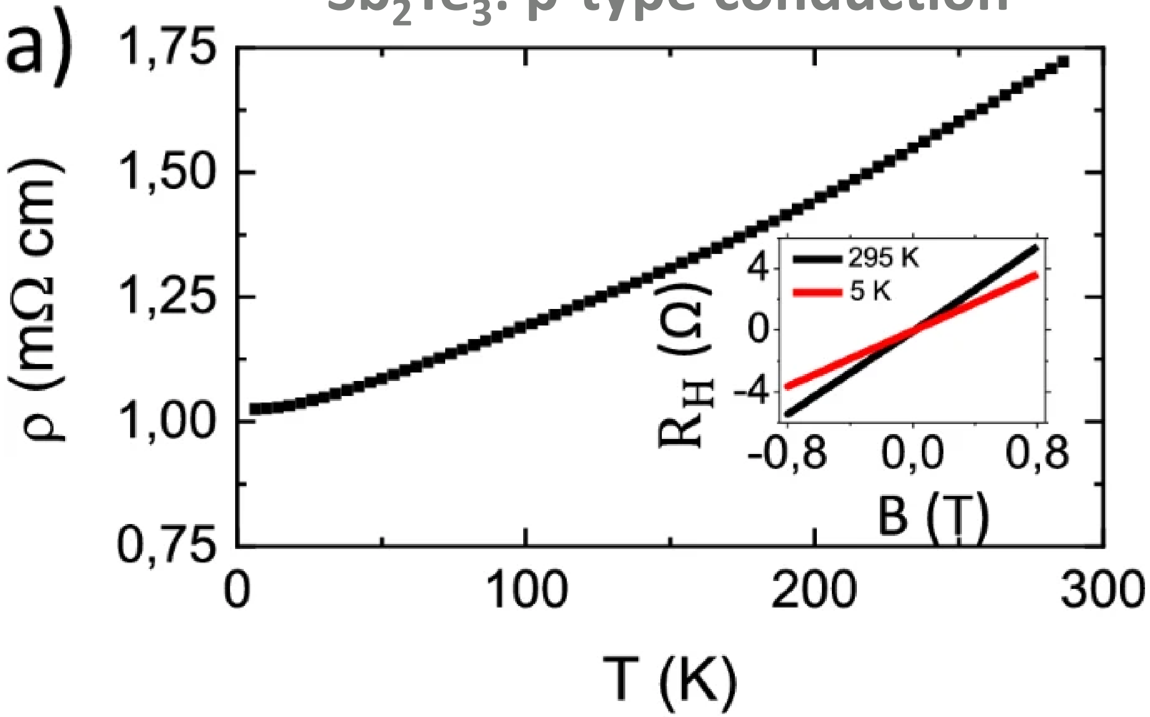

Bi_2Te_3: n-type conduction

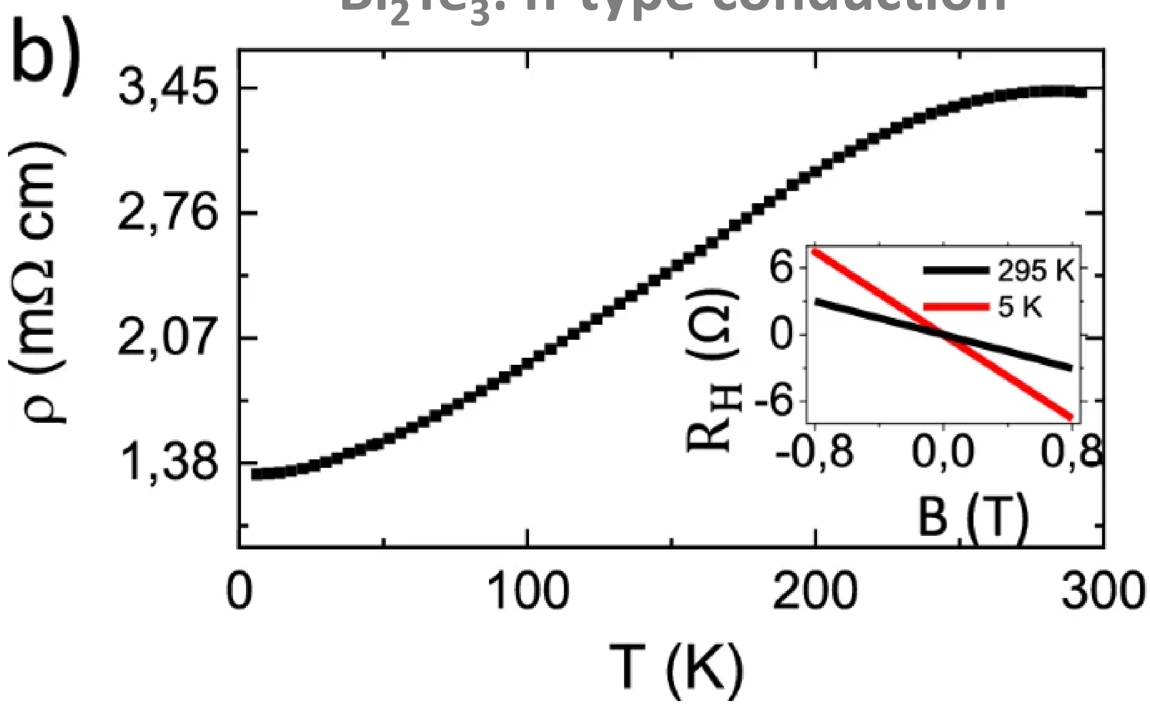

In both cases there is a relevant conduction from the bulk

L. Locatelli et al.,Sci. Rep. (2022)

Angular dependence

WAL ⟷ High mobility & High SOI ⟷ Conductive bulk, heavy elements

High mobility & High SOI ⟷ Topological channels ⟷ MC depends on perpendicular field

Sb_2Te_3

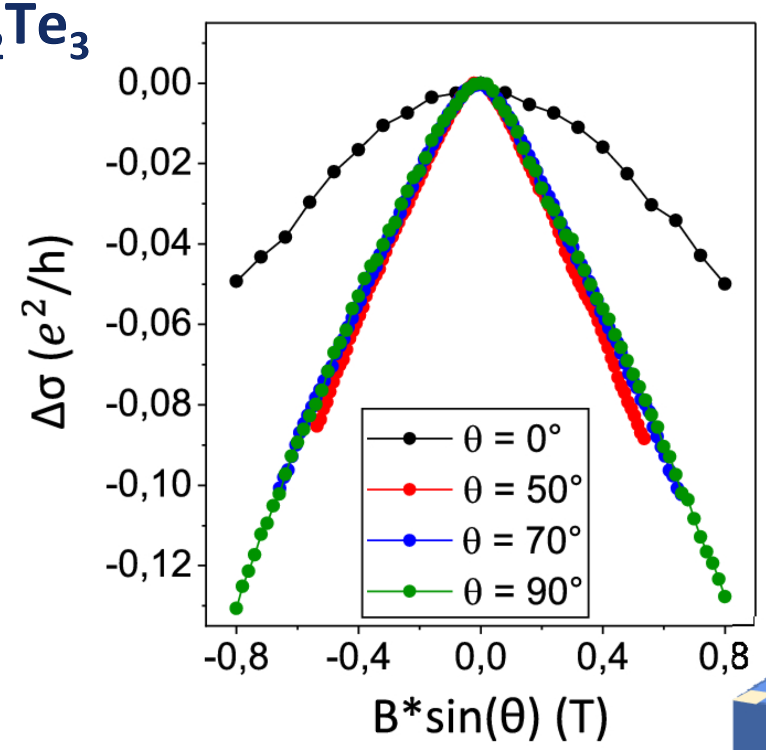

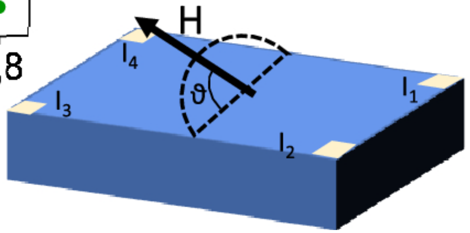

Bi_2Te_3

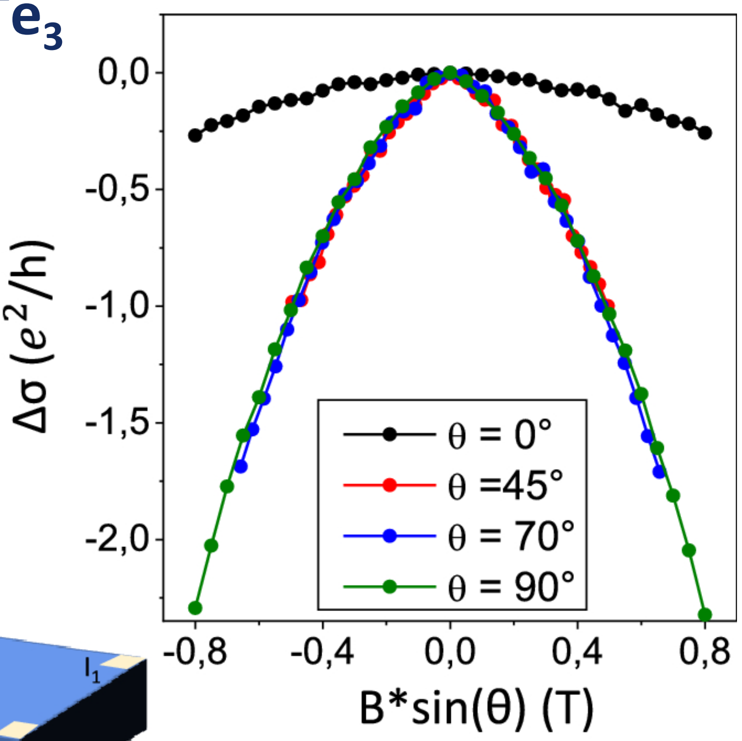

WAL origins from topological 2D-conduction

L. Locatelli et al.,Sci. Rep. (2022)